https://doi.org/10.5194/egusphere-2026-5233
Preprint. Discussion started: 14 September 2026

Influence of convective organization on the triple oxygen isotope composition of West African monsoon rainfall: insights from a 7-year record in Benin

Christine Vallet-Coulomb[1], Christophe Peugeot[2], Diego Chávez-Espinoza[1], Alexandre Zappelli[1], David Au Yang[1], Claudia Voigt[3], Alassane Abdoukarim[4], Valerie Kotchoni[4], Rita Houngue[5], Theodore Ouani[5], Simon Afouda[5], Maxime Wubda[5], Houégnon Géraud Vinel Gbewezoun[4], Anne Alexandre[1]

[1]Aix Marseille University, CNRS, IRD, INRA, Coll France, CEREGE, Aix-en-Provence, France

[2]Hydrosciences Montpellier, IRD, CNRS, University Montpellier, Montpellier, France

[3]Institute of Soil Sciences and Site Ecology, TU Dresden, 01737 Tharandt, Germany

[4]Laboratoire d'Hydrologie Appliquée, Abomey Calavi University, Benin

[5]IRD Bénin, Cotonou, Bénin

Correspondence to: Christine Vallet-Coulomb (vallet@cerege.fr)

Abstract. Triple oxygen isotopes, and specifically ^{17}O-excess, provide new opportunities to investigate kinetic fractionation associated with atmospheric moisture sources, continental moisture recycling, and cloud microphysical processes. However, observations of ^{17}O-excess in precipitation remain extremely scarce in Africa, leaving its potential for tracing atmospheric processes in the West African Monsoon (WAM) largely unexplored. Here we analyze a high-frequency precipitation isotope dataset (δ^{18}O, δ^{2}H, d-excess, and ^{17}O-excess) from Benin, comprising a 7-year record at the inland Nalohou station and a complementary 2-year record from a coastal station near Cotonou. Three isotopic clusters are identified inland, corresponding to distinct rainfall regimes. The first is associated with short-lived convective events affected by sub-cloud rain evaporation, while the second reflects more organized convective systems and a weak signature of continental moisture recycling. The third cluster, observed only inland, is characterized by strongly depleted δ^{18}O together with simultaneous decreases in d-excess and ^{17}O-excess, and occurs mainly during the mature monsoon stage. Its rainfall characteristics are consistent with larger and more organized convective systems, with a greater contribution from their stratiform component. At the interannual scale, δ^{18}O variability is more closely related to rainfall characteristics during the mature monsoon phase than to rainfall amount. Overall, these results indicate that, during the WAM mature monsoon phase, precipitation isotopes primarily reflect convective organization and associated cloud microphysical processes, while retaining a weak signature of continental moisture recycling during inland transport. These combined δ^{18}O, d-excess, and ^{17}O-excess data provide new observational constraints for isotope-enabled atmospheric and hydrological models.

https://doi.org/10.5194/egusphere-2026-5233
Preprint. Discussion started: 14 September 2026

1. Introduction

The West African Monsoon (WAM) is a major component of the tropical climate system and exerts a strong control on water resources, ecosystems, agriculture, and groundwater recharge across West Africa. The region has experienced marked hydroclimatic variability over recent decades, including severe droughts and flooding, shifts in rainfall seasonality, and an increasing trend in extreme precipitation (Biasutti, 2019; Chagnaud et al., 2024, 2022; Nicholson et al., 2018; Taylor et al., 2017). Understanding the mechanisms controlling rainfall variability within the WAM therefore remains a major scientific and societal challenge. Although the Sahel has received considerable attention due to the dramatic hydroclimatic fluctuations observed during the 20th century, particularly the severe droughts of the 1970s and 1980s (Giorgi, 2002; Hulme, 1992; Le Barbé et al., 2002; Mahamat Nour et al., 2023), the Sudanian climatic belt extending approximately between 5 and 10°N between the humid coastal domain and the semi-arid Sahel, has remained comparatively less studied (Galle et al., 2018; Nicholson et al., 2018). Despite relatively high annual rainfall totals, generally exceeding 1000 mm yr^{-1}, the region remains highly vulnerable to hydroclimatic variability because of strong seasonal contrasts in surface water availability, with major impacts on agriculture, water resources, and hydropower production. It also plays a key hydrological role within West Africa, as the WAM sustains the headwaters and discharge regimes of several major river systems, including the Niger, Volta, and Chari rivers.

The WAM results from complex interactions between large-scale atmospheric circulation, the seasonal migration of the Intertropical Convergence Zone (ITCZ), low-level monsoon flow from the tropical Atlantic Ocean, land–atmosphere feedbacks, and the activity of mesoscale convective systems (MCSs) (Lafore et al., 2011; Niang et al., 2020; Nicholson, 2013; Thorncroft et al., 2011). The ITCZ forms a major zone of convergence between dry continental air masses originating from the Sahara and moist monsoon air advected from the tropical Gulf of Guinea. Driven by the seasonal cycle of solar insolation, it migrates northward during boreal spring and summer and southward in autumn (Schneider et al., 2014). In response to this large-scale energetic forcing, the monsoon develops a well-defined tropical rain belt whose rainfall organization is strongly modulated by MCS activity and its interactions with land-surface conditions and regional atmospheric dynamics, including the African Easterly Jet (AEJ) and the Tropical Easterly Jet (TEJ). The rain belt migrates from the Guinean coastal region in March toward the Sahelian region in July–August, before retreating southward, while sustaining abundant rainfall over the Sudanian region from May–June to mid-October. During the mature phase of the monsoon in August, the main convective rain belt typically extends between approximately 5 and 15°N and is associated with widespread deep convection and intense MCS activity. At this stage, convective systems frequently span the entire tropospheric column, with cloud tops reaching the upper troposphere and extensive stratiform regions (Niang et al., 2020). Beyond this seasonal framework, interannual variability of the WAM rainfall is thought to arise from a combination of large-scale ocean–atmosphere interactions, including sea surface temperature gradients in the tropical Atlantic (Giannini et al., 2003), and land–atmosphere coupling processes related to soil moisture and surface conditions over the continent (Taylor et al., 2011).

Stable water isotopes in precipitation provide powerful integrative tracers of the atmospheric water cycle and have long been used to investigate hydrological and climatic processes across a wide range of spatial and temporal scales. The isotopic composition of rainfall reflects the combined influence of oceanic evaporation, atmospheric

https://doi.org/10.5194/egusphere-2026-5233
Preprint. Discussion started: 14 September 2026

transport, cloud microphysics, moisture recycling, and rain re-evaporation processes (Bailey et al., 2025; Fiorella et al., 2021; Yoshimura, 2015). In the WAM, these processes are tightly linked to the organization and intensity of convection, and precipitation isotopes therefore offer valuable insight into the functioning of monsoon systems and the dynamics of tropical rainfall (Nlend et al., 2020). Beyond their use as diagnostic tracers of present-day processes, stable water isotopes have also become an important constraint for isotope-enabled atmospheric general circulation models, providing a means to evaluate the representation of atmospheric moisture transport, convection, and cloud microphysics in numerical simulations (e.g. (Risi et al., 2010; Yoshimura et al., 2008)). By integrating the effects of multiple fractionation processes, isotopic data offer a physically based benchmark for assessing model performance and improving the representation of key processes governing the tropical hydrological cycle.

In tropical regions, rainfall $\delta^{18}O$ and $\delta^{2}H$ may show a negative relationship with precipitation amount, known as the “amount effect” (Dansgaard, 1964; Kurita et al., 2009; Rozanski et al., 1993), which has become a central framework for interpreting both modern precipitation variability and paleoclimate and paleohydrological archives such as speleothems or deep groundwaters (Jasechko and Taylor, 2015; Risi et al., 2023). However, the physical mechanisms underlying this relationship remain incompletely understood. Increasing evidence suggests that rainfall amount alone does not directly control isotopic depletion, but isotopes rather acts as an integrated proxy for convective organization, precipitation altitude, moisture transport, and cloud processes (Moore et al., 2014; Nlend et al., 2020; Scholl et al., 2009; Wei et al., 2018). In particular, the relative contributions of deep convection, stratiform precipitation, rain evaporation below cloud base, ice-phase processes, and event persistence may all influence precipitation isotopic signatures (Aggarwal et al., 2016; Tharammal et al., 2017; Yu et al., 2024). Understanding how these processes shape isotopic variability is therefore essential for improving both the interpretation of isotopes observations and the robustness of isotope-enabled climate simulations.

Beyond $\delta^{18}O$ and $\delta^{2}H$, second-order isotope parameters such as d-excess and ^{17}O-excess provide additional information on non-equilibrium fractionation processes occurring during evaporation and condensation. While d-excess has long been used to trace evaporation conditions at the moisture source, continental recycling and sub-cloud evaporation processes (Guan et al., 2013; Pfahl and Sodemann, 2014; Xia and Winnick, 2021), ^{17}O-excess has emerged more recently as a promising complementary tracer. Unlike d-excess, whose variability integrates both kinetic and temperature-dependent equilibrium effects, ^{17}O-excess is largely stripped of the temperature influence and therefore offers a more direct tool to isolate kinetic fractionation processes operating along the atmospheric water cycle. Theoretical and experimental studies suggest that ^{17}O-excess is particularly sensitive to humidity conditions during evaporation, rain evaporation below cloud base, vapor-liquid diffusive exchanges, and supersaturation effects associated with ice formation (Alexandre et al., 2025; Aron et al., 2020; He et al., 2021; Landais et al., 2010; Luz and Barkan, 2010; Risi et al., 2013; Surma et al., 2021; Voigt et al., 2026, 2022; Xia, 2023; Xia et al., 2023; Zhang et al., 2024). Consequently, ^{17}O-excess has the potential to provide complementary constraints on moisture sources, cloud microphysics and convective organization that cannot be resolved using $\delta^{18}O$ and $\delta^{2}H$ alone.

Despite this potential, observational ^{17}O-excess datasets remain scarce, particularly in tropical Africa. To date, very few studies have reported the triple oxygen isotope composition of precipitation isotopes within the WAM

https://doi.org/10.5194/egusphere-2026-5233
Preprint. Discussion started: 14 September 2026

(Alexandre et al., 2025; Landais et al., 2010; Terzer-Wassmuth et al., 2023). These studies provide descriptive observations of the seasonal variability of ^{17}O-excess. Among them, (Landais et al., 2010) interpreted the low ^{17}O-excess values observed in the Sahelian region as resulting primarily from rain re-evaporation, while not excluding the role of other atmospheric processes.

The present study investigates the drivers of precipitation isotope variability in the Sudanian region of the West African Monsoon, with particular emphasis on the information provided by triple oxygen isotopes composition. Due to its location between the humid Guinean coast and the semi-arid Sahel, the Sudanian zone occupies a key transitional position where changes in moisture transport, convective organization, and land–atmosphere interactions are expected to exert strong influences on precipitation isotopic composition. Unlike the Sahel, where rainfall is concentrated within a relatively short season, the Sudanian region experiences a longer monsoon cycle extending over approximately 6 months between April and October. This broader temporal window captures a wider diversity of convective regimes, offering a unique framework for investigating how monsoon evolution shapes precipitation isotopes. We analyze a multi-year, high frequency dataset of precipitation isotope composition (δ^{18}O, δ^{2}H, d-excess, and ^{17}O-excess) collected at two stations located along a coastal–continental transect in Benin, together with detailed rainfall and meteorological observations. By sampling precipitation along a common monsoon transport pathway but under contrasting continental influence, this observational design provides a natural framework for investigating how progressive inland transport and continental moisture recycling may influence precipitation isotopic composition. This unique dataset provides an opportunity to investigate how convective organization, expressed through different rainfall temporal structure, together with continental recycling, shape isotopic signatures across different monsoon regimes.

Specifically, this study aims to (i) identify the main controls on seasonal and event-scale isotopic variability in the WAM region, (ii) assess the respective roles of vapor sources, convective organization, and associated cloud microphysical processes governing condensation and evaporation, in shaping δ^{18}O, d-excess, and ^{17}O-excess signatures, and (iii) evaluate the added-value of ^{17}O-excess for tracing atmospheric humidity, moisture recycling, and cloud microphysical processes. More broadly, this work seeks to improve the process-based understanding of tropical precipitation isotopes and to provide new observational constraints for isotope-enabled atmospheric, paleoclimate and hydrological applications.

2. Data acquisition and methods

2.1 Rainfall sampling stations

Both monitoring stations are located along the West African monsoon inflow and are therefore influenced by the same large-scale monsoon circulation (Figure 1). The coastal station (6.42°N, 2.34°E, altitude around 10 m) is located on the Campus of the University of Abomey-Calavi, approximately 8 km from the Gulf of Guinea Coast. This station will be further designated as the coastal station. The Nalohou station (9.743N, 1.606E, altitude 500 m) is situated approximately 400 km inland in the Sudanian climatic zone, and will be further designated as the inland station. Although both stations are influenced by the same monsoon system, they experience contrasting rainfall regimes associated with the seasonal migration of the Intertropical Convergence Zone: a bimodal regime

https://doi.org/10.5194/egusphere-2026-5233
Preprint. Discussion started: 14 September 2026

at the coast, and a unimodal monsoon regime inland (Aïzansi et al., 2024; Nicholson et al., 2018). Together, the two stations provide a coastal-inland transect suitable for investigating isotopic variations across contrasting climatic settings.

Two PALMEX rain collectors (Gröning et al., 2012) were installed in 2018. At the coastal station, the sampling was performed weekly from June 2018 to October 2019. At the inland station, the sampling was conducted at a quasi-event time step from April 2018 until the end of the 2024 season. Samples were stored in 30 mL brown glass vials, completely filled to avoid air bubble, tightly sealed, and wrapped with Parafilm before shipment to France.

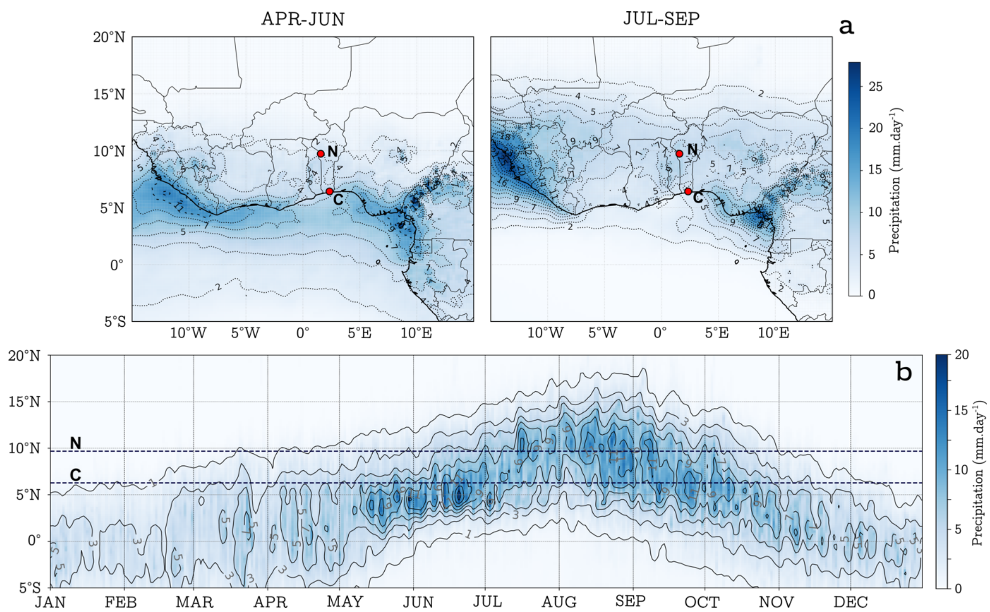

Figure 1: Mean precipitation patterns over West Africa derived from the ERA5 hourly reanalysis dataset (Hersbach, et al., 2023) for the period 2018-2024. (a) Mean daily precipitation during April-June (left) and July-September (right). Red points indicate the locations of the two sampling stations. (b) Hovmöller diagram of daily precipitation averaged between 15°W and 15°E for the period 2018-2024, shown as a function of latitude from 5°S to 20°N. Black dashed horizontal lines indicate the latitudes of the two sampling stations.

2.2 Isotopic analysis

The isotopic composition of water (δ^2H, δ^{18}O and ^{17}O-excess was measured at CEREGE using a Wavelength-scanned Cavity Ring-Down Spectrometer (WS-CRDS L2140-i, Picarro Inc., California, USA). Four in-house laboratory reference waters (working standards WS) calibrated against the international primary reference waters VSMOW2 and SLAP2, were used. Three WS were used for normalization, and one was dedicated to quality assurance and quality control (QA/QC). Three replicates of the QA/QC standard (in 3 different vials) were distributed throughout each analytical run: one after the first set of normalization standards, and the other two randomly among the samples. A minimum of three replicates was analyzed for each rainfall sample, with eight injection per replicate. The run sequence was designed to minimize the memory effects and compensate for potential instrumental drift. In addition, a memory correction was applied during post-processing. The first injections were discarded, and the mean of the six last injections was retained. Data were normalized to the VSMOW-SLAP scale using the two sets of WS that bracket the measurement runs. The full analytical protocol and post-measurement data processing is described in detail in (Vallet-Coulomb et al., 2021).

We use a $\delta^{17}O$ value of –26.6968‰ for SLAP (Schoenemann et al., 2013) for normalization. ^{17}O-excess values were determined from the following equation:

$$^{17}\text{O-excess} = \ln(\delta^{17}\text{O} + 1) - 0.528 \times \ln(\delta^{18}\text{O} + 1) \qquad (1)$$

where ^{17}O-excess is expressed in per meg (10^{-6}).

A total of 295 and 52 samples were collected and analyzed at the inland and coastal stations, respectively. Long-term analytical performance was assessed using QA/QC statistics from all measurement runs (n = 38 for this study). The SD of the QA/QC was 0.05‰, 0.33‰ and 5 per meg for $\delta^{2}H$, $\delta^{18}O$ and ^{17}O-excess, respectively. The deviation from the assigned value was 0.03‰, -0.06‰ and 0 per meg for $\delta^{2}H$, $\delta^{18}O$ and ^{17}O-excess, respectively. Additionally, for each rainfall sample, the standard deviation of ^{17}O-excess was calculated from its three replicate measurements. The average of these sample-level standard deviations was 7 +/- 3 per meg.

2.3 Precipitation and meteorological data

2.3.1 Data sources

In Northern Benin, precipitation is routinely measured at different stations by the AMMA-CATCH Observatory (Galle et al., 2018), at 5-minute intervals using a tipping bucket rain gauge and subsequently averaged to hourly values. We used precipitation data from the Inland 3 station (40 m far from the sampling station) at both hourly and 5-minute time scales. Additionally, precipitation data from the Inland 2 station (1950 m far from the sampling station) were used for to fill gaps in the hourly time series (11.2% of gaps in 2020 and 0.7 % in 2023). The resulting complete hourly time series was then used to associate a precipitation volume with each isotope sample.

In addition, meteorological data were obtained from the station Nalo-Flux station (AMMA-CATCH Observatory, located 280 m far from the sampling station): air temperature (Ta), relative humidity (RH) and wind speed (WSpd). All variables were measured 2 m above ground level (agl) at 5-minute intervals and subsequently average to 30-minute values.

Outgoing longwave radiation (OLR) hourly data, as a proxy of convective intensity, were obtained from the ERA5 dataset (Hersbach, H. et al., 2023).

At the coastal site, we used the 2015-2019 daily precipitation data from the International Institute of Tropical Agriculture (IITA) station (6.42°N, 2.33°E, altitude 14 m), located approximately 2 km far from the sampling station, to calculate amount-weighted mean compositions.

https://doi.org/10.5194/egusphere-2026-5233
Preprint. Discussion started: 14 September 2026

2.3.2 Rainfall characteristics

Rainfall characteristics are described using complementary metrics derived from two dataset temporal resolutions (hourly and 5-min). Hourly data were used to derive metrics describing rainfall intensity and persistence within each day. For each wet day (P>0 mm), we computed (i) the mean hourly rainfall intensity considering non-zero hourly values (mm h^{-1}), (ii) the daily rainfall duration (number of rainy hours per rainy day), and (iii) the fraction of daily rainfall associated with weak intensities (weak rainfall fraction), weak intensities being defined relative to the median of the hourly rainfall distribution over the whole period.

To characterize rainfall organization at finer temporal scale, we used the 5-min precipitation data to identify rainfall events, defined here as continuous sequences of non-zero rainfall separated by at least 30 minutes without precipitation. For each day, we computed (i) the mean event duration (min), and (ii) the mean event intensity (converted to mm h^{-1}).

2.3.3 Monsoon phase identification from cumulative precipitation

To characterize intra-seasonal dynamics of the WAM at the inland station, we analyzed daily cumulative precipitation (Pcum) for each year of the 2018-2024 period. Visual inspection of annual Pcum curves consistently revealed a two-phase behavior within the monsoon season that was well represented by a single breakpoint, with an initial slow accumulation phase, followed by a faster accumulation phase. Motivated by this systematic pattern, we applied a piecewise linear regression to identify the transition between these two phases. The analysis was restricted to the monsoon season, defined as starting on the first day when cumulative precipitation exceeded 5 mm and ending on the first day after September 30th followed a 10-day period with less than 5 mm. This criterion excludes isolated rainfall events that may occur after the seasonal weakening of the monsoon. Within this monsoon period, the optimal breakpoint was defined as the point minimizing the combined residual sum of squares of the two fitted regression segments, considering a minimum of 20 daily observations on each side of the breakpoint to ensure robust estimation of both regression segments.

The annual characteristics of both phases, including timing (start and end dates), duration (days), total precipitation (mm), and regression slope (mm day^{-1}), which represents the mean daily precipitation accumulation rate, were calculated for each phase. This approach provides an objective, reproducible, and site-specific characterization of changes in rainfall accumulation regimes during the monsoon season.

2.4 Moisture source analysis from HYSPLIT back trajectories

Moisture source regions were identified by using a back trajectory analysis. We used the Hybrid Single-particle Lagrangian Integrated Trajectory (HYSPLIT) modeling of the Air Resources Laboratory (ARL) of the National Oceanic and Atmospheric Administration (NOAA) (Stein et al., 2015) to generate trajectories. The Global Data Assimilation System (GDAS1) archive database of NCAR/NCEP, with a spatial resolution of 1°×1°, was used as meteorological input data (available at https://www.ready.noaa.gov/data/archives/gdas1/).

https://doi.org/10.5194/egusphere-2026-5233
Preprint. Discussion started: 14 September 2026

The altitude at which the backwards trajectories were initialized was determined from the lifting condensation level (LCL), which provides a reasonable approximation of the cloud base height. Daily mean LCL values were calculated daily from ERA5 data following (Romps, 2017), providing mean LCL altitudes of 906 ± 394 m for April-May, and 388 ± 39 m for June-October over 2018-2024 at the inland site, and pretty similar values at the coastal site. At both sites, backwards trajectories were therefore initialized every 6 hours at 1000 m agl and 500 m agl for these two periods, respectively. Trajectories were extracted for a duration of 7 days (168 hours), starting from the location of the inland (April-October over 2018 – 2024) and coastal (May-October over 2018-2019) stations. Trajectory duration (7 days) was chosen as a reasonable duration to fit within the 10-day average residence time of water vapor in the atmosphere, but avoiding too long trajectories because their uncertainty increases with time. All calculations were performed using the PySPLIT package (Warner, 2018), which is a Python-based Application Programming Interface (API) for HYSPLIT.

Rainy trajectories were selected (P>0 for the last 6 hours of the trajectories prior to arrival at the target site). Moisture source areas were identified using changes in specific humidity along each trajectory, following the method proposed by (Sodemann et al., 2008), and further used in different studies (Cai et al., 2018; Hassenruck-Gudipati et al., 2023; Zhan et al., 2023). Moisture uptake was calculated every 6 hours along each trajectory based on changes in specific humidity, using thresholds of +0.2 for evaporation and - 0.2 for precipitation. Uptake was attributed to surface evaporation only when the trajectory was located below the boundary layer, as defined by the boundary layer height in the HYSPLIT model. The total moisture uptake was partitioned into contributions from surface evaporation, above-boundary-layer moisture sources, and non-attributed fractions (Sodemann et al., 2008). The latter represents moisture contributions that cannot be uniquely assigned to either surface or free-atmosphere sources by the attribution procedure. Surface uptake fractions were then progressively adjusted along each trajectory (following forward time steps towards the target station) to account for successive gains and losses of atmospheric moisture associated with evaporation and precipitation processes. These dimensionless fractions were subsequently weighted by the precipitation accumulated during the last 6 hours prior to arrival at the target site, yielding the amount of precipitation (mm) attributed to each surface moisture uptake event along the trajectory. For each trajectory group, these attributed precipitation amounts were aggregated within 1° x 1° grid cells. Grid cell totals were finally normalized by the total precipitation of the trajectory group, so that the resulting values represent the fractional contribution of each source region to the of total precipitation.

2.5 Definition of isotopic clusters

A cluster analysis based on $\delta^{18}O$, d-excess, and ^{17}O-excess was applied to the isotopic dataset at both stations. Prior to clustering, $\delta^{18}O$, d-excess, and ^{17}O-excess were standardized using a z-score transformation, by subtracting the mean and dividing by the standard deviation of each variable, using the StandardScaler function from the Python scikit-learn library (Pedregosa et al., 2011). This step ensures that all isotopic variables contribute equally to the Euclidean distance used in the clustering procedure. The clustering was performed using the k-means algorithm implemented in scikit-learn, which partitions the dataset into k groups by minimizing the within-cluster sum of squared distances (inertia) (Lloyd, 1982). The optimal number of clusters was determined using the elbow method (Thorndike, 1953), based on the decrease in inertia for k values ranging from 1 to 9. The k-means algorithm was then run with multiple initializations (n = 10) and a fixed random seed to ensure reproducibility. Finallyn cluster

https://doi.org/10.5194/egusphere-2026-5233
Preprint. Discussion started: 14 September 2026

separation was evaluated using the silhouette coefficient (Rousseeuw, 1987), which measures the degree of separation between clusters by comparing within-cluster cohesion to the distance from the nearest neighboring cluster.

3. Results

Given the contrasting data availability – seven years of continuous isotope and meteorological measurements at the inland station versus only two years of isotopes measurements and daily precipitation data at the coastal station – we adopt a dual approach: comparing moisture sources and seasonal isotope patterns across both stations, and using the longer inland record to characterize rainfall regimes and their isotopic signatures, and to assess intraseasonal and interannual variability through statistical analyses.

3.1 Moisture sources

Back-trajectory analysis identifies the dominant regional transport pathways of air masses associated with precipitation at both stations and the main regions of moisture uptake represented by the GDAS reanalysis. These pathways are predominantly linked to tropical Atlantic regions, with additional contributions from continental areas for the inland site (Figure 2).

At the coastal station, moisture uptake is essentially oceanic, with a relatively homogeneous distribution of sources along the air-mass trajectories extending from approximately 20°S to the Gulf of Guinea coast. Monthly variations (Figure A1) show no clear seasonal evolution of the source areas. In the southern part of the trajectories, the mean flow is oriented toward the north-northwest, followed by a marked deflection toward the northeast after crossing the equator, under the influence of the Coriolis effect.

At the inland site, the dominant regional transport pathways remain largely oceanic and are similar to those at the coastal site, but with an additional, spatially concentrated continental contribution. This contribution is located over central Ghana, in the Lake Volta region. A small fraction of the surface moisture also arrives from the east, potentially associated with the East African Jet. Monthly variations (Figure A2) indicate no marked seasonal variation in the oceanic source regions, whereas continental moisture uptake over southern Ghana is particularly concentrated between July and October, *i.e.* the most rainy months. In contrast, the eastern moisture contribution is absent during July–August, when transport is largely dominated by the oceanic flow.

https://doi.org/10.5194/egusphere-2026-5233
Preprint. Discussion started: 14 September 2026

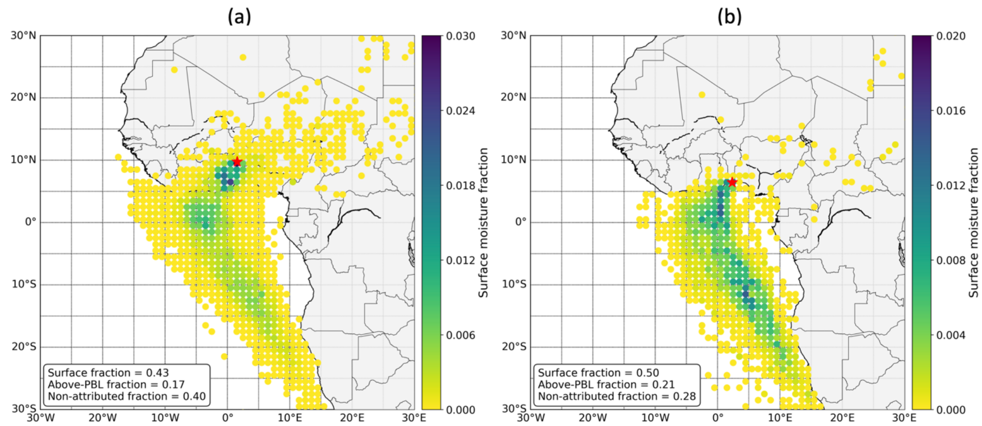

Figure 2: Surface moisture source regions derived from back-trajectory analysis, expressed as the rainfall-weighted fraction of surface moisture contribution at the target site. The inset reports the fractions of moisture uptake attributed to surface evaporation, above-PBL sources, and non-attributed sources (see Methods for details). Results are averaged over all months and years of the study period. Back-trajectories were computed using the HYSPLIT model with GDAS reanalysis data. All calculations were performed with the PySPLIT package (Warner, 2018).

3.2 Hydroclimatic and isotopic dataset

3.2.1 Isotopic compositions and local meteoric water lines

At the inland station, a total of 295 quasi-event samples were collected and analyzed, representing approximately 96% of the total rainfall. Unsampled events were generally small and isolated, occurring at the beginning of the rainy season. A small number of samples (n = 7) exhibited clear evaporated signature (d-excess <0) and were considered as outliers and discarded. The remaining 288 samples represent 94% of the total rainfall, with the proportion of unsampled precipitations varying between 1 and 9 % depending on the year, and essentially occurring during the first phase of the monsoon season. The amount-weighted mean isotopic compositions is $\delta^{18}O$ = -4.61 ‰, $\delta^{2}H$ = -24.99 ‰, ^{17}O-excess = 20 per meg, and d-excess = 11.90 ‰.

At the coastal station, a total of 52 samples (7-day time step) samples were collected. The amount-weighted mean isotopic compositions is $\delta^{18}O$ = -3.55 ‰, $\delta^{2}H$ = -27.32 ‰, ^{17}O-excess = 14 per meg, and d-excess = 11.07 ‰. The local meteoric water lines (Figure A3) are very similar between the two stations for $\delta^{18}O$- $\delta^{2}H$, while the slope between $\delta^{17}O'$ and $\delta^{18}O'$ was 0.5266 and 0.5250 at the inland and coastal stations, respectively.

3.2.2 Average seasonal cycles

Over their respective sampling periods, mean annual precipitation was 1337 mm at the coastal station (2018-2019) and 1527 mm at the inland station (2018-2024), with markedly different seasonal distributions (Figure 3). The

https://doi.org/10.5194/egusphere-2026-5233
Preprint. Discussion started: 14 September 2026

coastal station exhibits a bimodal rainfall regime, with two precipitation maxima in May-June and September-October separated by a short dry period in July-August. In contrast, precipitation at the inland station increases progressively from March to June, followed by a broad rainfall maximum extending until the retreat of the rainy season in October, resulting in a unimodal rainfall regime. These contrasting seasonal patterns are consistent with the regional rainfall patterns over West Africa (Nicholson et al., 2018), with the northward migration of the rain belt from the Gulf of Guinean region towards the Sahel between March and August, followed by its southward return in September-October (Figure 1).

At both sites, precipitation exhibits a pronounced seasonal cycle in $\delta^{18}O$, d-excess and ^{17}O-excess, with each tracer displaying a distinct temporal evolution (Figure 3). The $\delta^{18}O$ values show a marked seasonal depletion during the monsoon period at both stations, with the lowest values occurring during the core monsoon rainfall. The seasonal amplitude of $\delta^{18}O$ is larger inland than at the coastal site, and a W-shape seasonal pattern is observed at both sites. At the coastal site, this pattern corresponds to the bimodal rainfall regime, while inland, the two minima (early July and early September, Figure 3) are not associated with a decrease in precipitation. A similar pattern has been reported for Douala, in Cameroon (Nlend et al 2020), and attributed to strong convective activity along air mass trajectories. d-excess values display its lowest values during periods of low rainfall. However, their maximum values, observed in May at the inland site and March-April at the coastal site, do not coincide with rainfall peaks. ^{17}O-excess exhibits broadly a similar pattern, with lowest values also occurring during the low rainfall periods. Overall, ^{17}O-excess values are generally higher inland than at the coastal site.

Monthly data from the Global Network of isotopes in Precipitation (GNIP) database for the GNIP Cotonou station over 2015–2018 fall within the range of variability observed in this study and reproduce the main features of the seasonal isotopic cycle, supporting the representativeness of the present dataset.

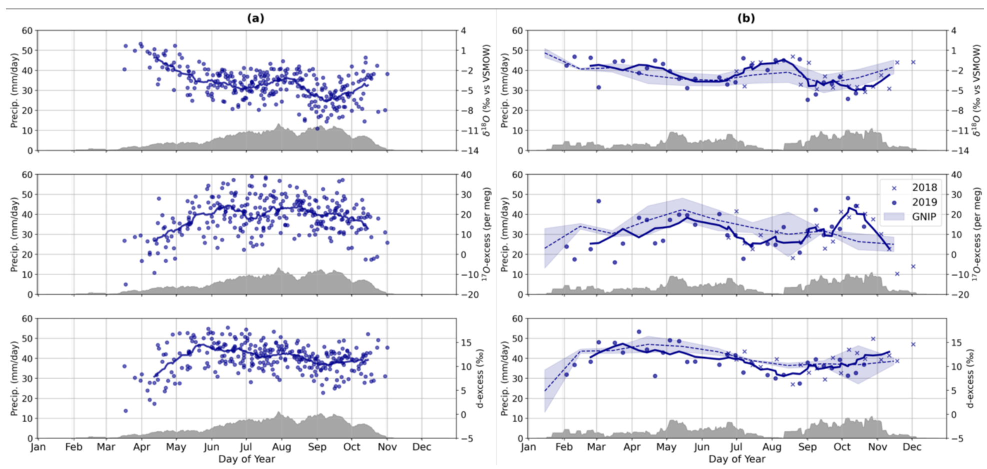

Figure 3: Seasonal evolution of isotopic composition ($\delta^{18}O$, d-excess, ^{17}O-excess) and precipitation at both sites over their respective monitoring periods: 2018–2024 for the inland station (a: Nalohou) 2018–2019 for the coastal station (b: Cotonou). Smoothed mean isotopic values (bold lines) are calculated over 15 (inland) and 5 (coastal) consecutive data points. The GNIP reference dataset from Cotonou (Terzer-Wassmuth et al., 2023) is shown as

https://doi.org/10.5194/egusphere-2026-5233
Preprint. Discussion started: 14 September 2026

monthly means over 2015–2018 (dotted lines) with standard deviation indicated by shaded areas. Corresponding precipitation seasonal cycles are shown as 15-day rolling averages.

3.2.3 Relationships between $\delta^{18}O$ and precipitation amounts

The relationship between precipitation amounts and $\delta^{18}O$ was examined to assess the presence of the "amount effect" at the inland site. At the sample scale (Figure 4a), $\delta^{18}O$ showed a weak negative correlation with sampled precipitation amount ($r = -0.248$, $p < 0.001$), indicating that precipitation amount explains only a small fraction of the isotopic variability ($R^2 = 0.062$). At the annual scale (Figure 4b), no correlation is observed ($r = -0.377$, $p = 0.40$), and the three wettest years (2018, 2019 and 2023) show the widest range of $\delta^{18}O$ values. At the monthly scale (Figure 4c), a significant negative correlation between $\delta^{18}O$ and precipitation was observed for months with total precipitation below 200 mm ($r = -0.708$, $p < 0.001$). In contrast, no relationship was detected for months with precipitation exceeding 200 mm ($r = -0.079$, $p = 0.7$), corresponding to the June-September period, which account for more than 70% of the total annual rainfall (Figure 4d). This indicates that a simple amount effect is not a dominant control on isotopic composition for the core of the rainy season over the studied period.

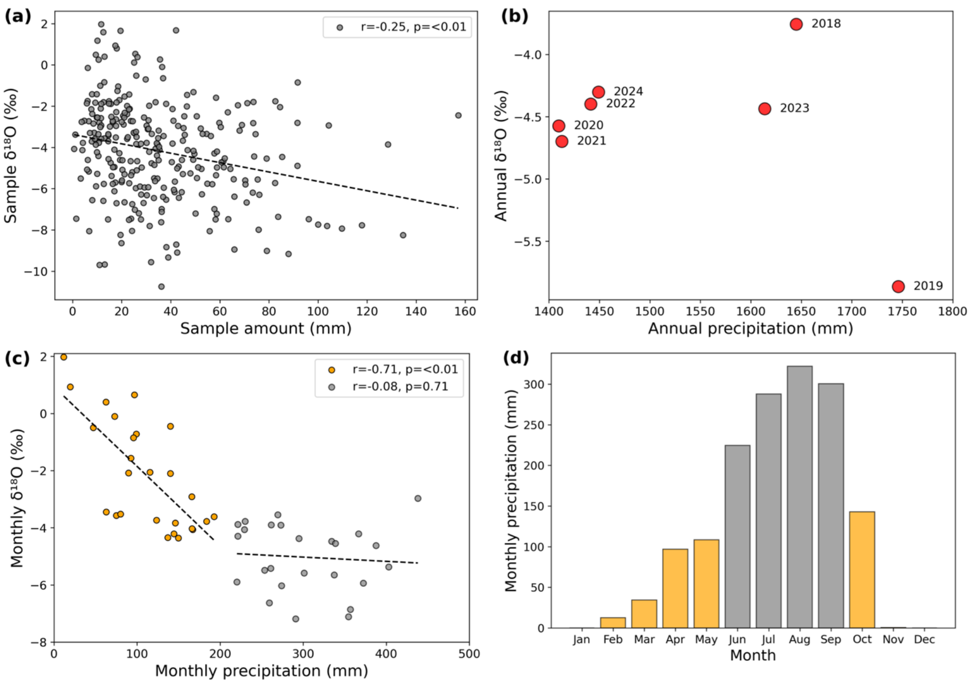

Figure 4: Relationship between precipitation amount and $\delta^{18}O$ at sample (a), annual (b) and monthly (c) time scales. At the monthly time scale, orange dots correspond to the months with precipitation amounts < 200 mm (February to May and October, accounting for 28 % of annual rainfall), whereas black dots correspond to the months with precipitation amounts > 200 mm (June to September, accounting for 72% of annual rainfall). Mean

https://doi.org/10.5194/egusphere-2026-5233
Preprint. Discussion started: 14 September 2026

monthly rainfall amounts using the same color code is shown in (d). Linear regression lines are shown as dotted lines, and Pearson correlation coefficients (r) and associated p-values are reported.

3.3 Isotope-based cluster analysis

3.3.1 Composition of isotopic clusters

Three clusters were obtained at the inland site and two clusters at the coastal site. In the isotopic space defined by $\delta^{18}O$, d-excess, and ^{17}O-excess (Figures 5 and 6a), the resulting clusters show partial overlap (mean silhouette scores = 0.307 and 0.402 for the inland and coastal sites, respectively), while remaining sufficiently distinct to support the identification of coherent isotopic characteristics.

At the inland site, the first cluster is characterized by relatively high $\delta^{18}O$ values (-1.6‰) associated with low d-excess (8.8 ‰) and low ^{17}O-excess (7 per meg). The second cluster exhibits more depleted $\delta^{18}O$ values (-3.6 ‰) together with higher ^{17}O-excess and d-excess (24 per meg and 13.7 ‰, respectively). The third cluster shows strongly depleted $\delta^{18}O$ values (-6.6 ‰) combined with intermediate values of ^{17}O-excess and d-excess (20 per meg and 10.7 ‰, respectively). The difference in mean ^{17}O-excess between C2 and C3 is 4 per meg (with similar values obtained using both unweighted and amount-weighted averages). To evaluate the robustness of this difference with respect to analytical uncertainty, a Monte Carlo uncertainty propagation was performed. For each cluster, individual ^{17}O-excess values were independently perturbed, assuming a Gaussian analytical uncertainty, estimated from the standard deviation of 7 per meg (see section 2.2), and cluster mean values were recomputed over 10000 realizations. The resulting distribution of differences between cluster means (C2 − C3) remained consistently positive, yielding a 95% confidence interval that did not include zero and a probability P(C2 > C3) equal to 1.0 (Figure A4).

At the coastal site, isotopic compositions span a narrower range and the strongly $\delta^{18}O$-depleted compositions observed inland (cluster 3) are absent. The first cluster is very similar to its inland counterpart, with an enriched $\delta^{18}O$ mean (-0.8 ‰) associated with low ^{17}O-excess (3 per meg), and moderately low d-excess (9.9 ‰). The second cluster exhibits lower ^{17}O-excess and d-excess (16 per meg and 11.9 ‰, respectively) than its inland counterpart, despite similar $\delta^{18}O$ (-4.0 ‰). Overall, the dataset highlights a general inland shift toward lower $\delta^{18}O$ values and higher ^{17}O-excess and d-excess.

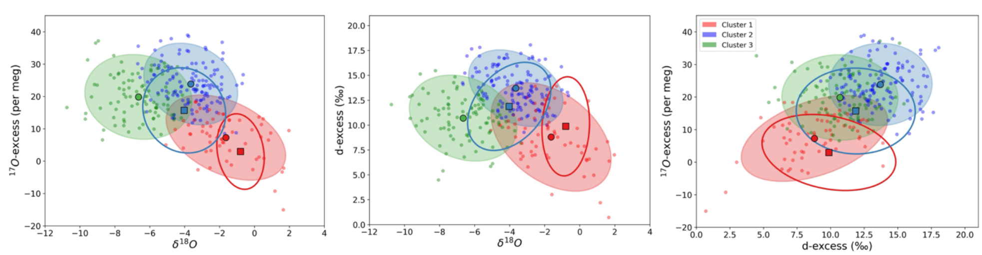

Figure 5: Bivariate plots of isotopic compositions per cluster, showing covariance ellipses (2σ) and cluster mean values. For the inland station, both ellipses and individual data points are shown. For the coastal station, only the

https://doi.org/10.5194/egusphere-2026-5233
Preprint. Discussion started: 14 September 2026

ellipses and cluster mean values are displayed for clarity. Clusters C1 are shown in red, Clusters C2 in blue, and Cluster C3, present only at the inland station, in green.

3.3.2 Meteorological characteristics of isotopic clusters at the inland site

At the inland site, Cluster 1 (C1) represents 15% of mean annual rainfall, while Cluster 2 and 3 (C2 and C3) share the majority of rainfall (47 and 38 %, respectively). The three isotopic clusters display distinct rainfall characteristics in terms of intensity and event duration (Figure 6b). C1 is characterized by relatively high event-scale intensities (11.5 mm h^{-1}) and the shortest mean event durations (68 min). At hourly resolution, however, this distinction disappears, as many events have durations close to one hour, and the highest hourly mean intensity (5.3 mm h^{-1}) is observed for C2. In contrast, Cluster C3 is characterized by lower rainfall intensities at both hourly (3.9 mm h^{-1}) and event (7.2 mm h^{-1}) scales, despite the occurrence of some intense outliers. Event durations are broadly similar for C2 and C3, whereas daily rainfall duration are higher for C3 (4.3 h day^{-1}) than C2 (3.8 h day^{-1}). In addition, C3 displays the highest fraction of weak rainfall contributions, with 28 % of rainfall below the median intensity threshold, compared with 19 % and 18 % for C1 and C2, respectively. Together with its longer rain duration, this pattern is consistent with more persistent rainfall conditions and a greater contribution of low-to-moderate intensity precipitation. Median values are consistent with these patterns.

Daily meteorological conditions (Figure 6c) further distinguish the three clusters. C1 corresponds to the driest (RH = 70.7 %) and warmest (Ta = 25.2 °C) conditions, with relatively higher OLR (239 W m^{-2}) than C2 and C3 (226 W m^{-2} and 220 W m^{-2}, respectively). The coolest and most humid conditions are observed for C3, which also has the lowest OLR. Wind speed is lowest for C3 (1.1 m s^{-1}), whereas C1 exhibits the greatest variability in wind speed, with an mean value (1.2 m s^{-1}) similar to that of C2. C1 also exhibits the widest range of relative humidity values among the three clusters. To assess whether this variability is reflected in isotopic composition, relationships between isotopic composition and RH were further examined. Both ^{17}O-excess and d-excess showed modest positive correlations with RH (Pearson $r = 0.35$, $p = 0.006$ and $r = 0.41$, $p = 0.001$, respectively with $n = 61$), whereas $\delta^{18}O$ showed a strong negative correlation ($r = -0.73$, $p < 0.001$).

Overall, precipitation characteristics and daily meteorological conditions show consistent differences among isotopic clusters, indicating distinct rainfall regimes. C1 corresponds to short rainfall events under relatively dry conditions, C2 to more intense rainfall, and C3 to lower-intensity and more persistent rainfall.

https://doi.org/10.5194/egusphere-2026-5233
Preprint. Discussion started: 14 September 2026

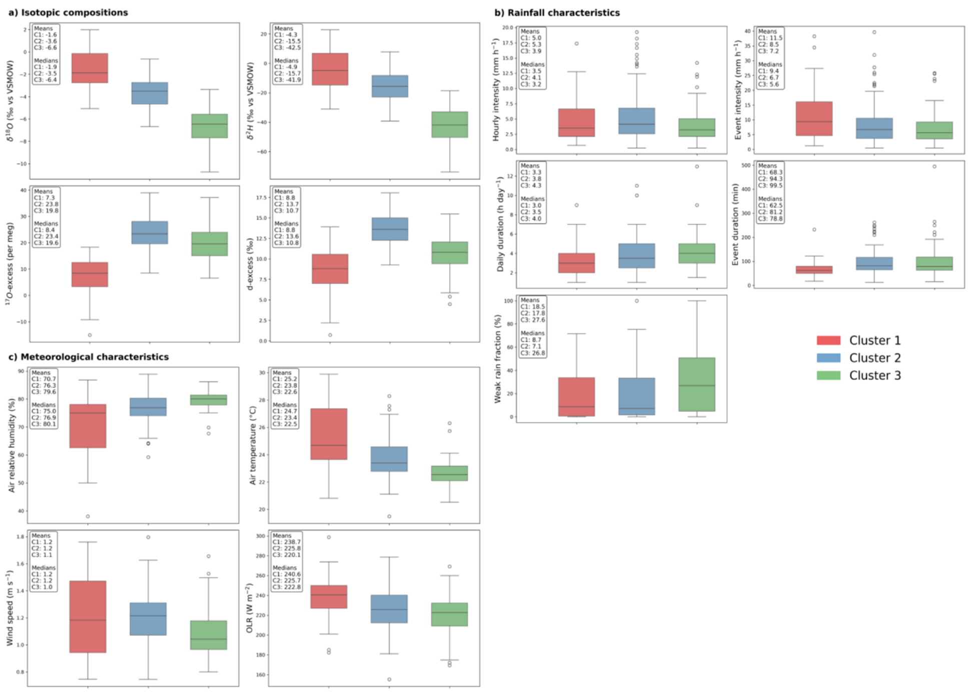

Figure 6: Boxplots per cluster at the inland site representing (a) isotopic compositions; (b) rainfall characteristics: hourly intensity (mm h-1); event intensity (mm h-1); daily rainfall duration (h day-1); event duration (min); weak rain fraction (%); (c) meteorological variables: relative humidity (%); air temperature (°C); wind speed (m s^{-1}); outgoing longwave radiation (W m^{-2}) as a proxy for convective activity. For rainfall and meteorological variables, each metric is the mean of rainy days during the period covered by each individual isotope sample, considering up to the last five days (see section 2). All average values are also provided in the inserted legends.

3.3.3 Seasonal distribution of isotopic clusters at the inland site

The relative contributions of the clusters vary markedly during the rainfall season (Figure 7), indicating that these rainfall/isotopic regimes are not randomly distributed throughout the rainy season. During the early monsoon phase, until the beginning of May, C1 dominates, while C2 and C3 contribute only marginally. From early May to mid-August, C2 becomes dominant. After mid-August, the contribution of the C3 increases sharply and dominates until the end of the monsoon retreat, while C1 reappears at the end of the season. The pronounced seasonal organization of isotopic clusters indicates that observed the sub-seasonal isotopic variability is closely associated with the seasonal evolution of the monsoon system.

https://doi.org/10.5194/egusphere-2026-5233
Preprint. Discussion started: 14 September 2026

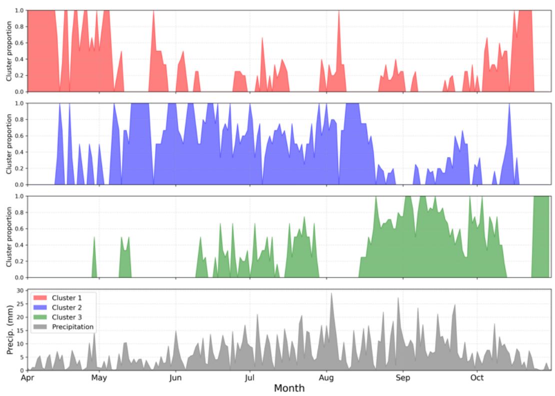

Figure 7: Daily proportions of cluster occurrences over the monsoon season at the inland site over 2018-2024.

3.4 Interannual variations of the two-phase structure of the monsoon season

3.4.1 Monsoon phases and associated rainfall characteristics

Given the structuration of isotopic compositions and associated meteorological regimes revealed by the cluster analysis (Figure 5 and 6), and the seasonal trend in cluster proportions (Figure 7), we investigate whether this organization is reflected in seasonal precipitation characteristics and how it relates to interannual variability. To this end, each monsoon season was divided into two phases, based on annual cumulative precipitation curves (see section 2.3.3). The transition between these two phases is identified for each year, and further referred to as a pre-onset phase and a core monsoon phase (Figure 8). Significant variations are found for the timing of the transition (21 May to 26 June; mean: 8 June, DOY = 159), and for that of the first significant rainfall events, ranging from 9 February (2024) to 16 April (2021). The monsoon retreat occurs between 15 and 30 October.

The two phases differ markedly in their mean rainfall characteristics. The pre-onset phase is associated with lower mean daily accumulation rates (3.2 ± 1.0 mm day^{-1}, n = 7) and contributes to a limited fraction of annual precipitation, ranging from 11 to 25% (mean ~18%). In contrast, the core monsoon phase is characterized by higher mean daily accumulation rates (10.1 ± 2 mm day^{-1}, n = 7) and accounts for the majority of annual rainfall.

Relationships between annual characteristics of the two phases were assessed using the non-parametric Spearman rank correlation (Figure 9), which is better suited to small sample sizes (n = 7 years) and less sensitive to outliers than Pearson correlation. Annual precipitation is strongly correlated with precipitation amount and accumulation rate during the pre-onset phase ($r_s = 0.89$ and 0.82, respectively), as well as with the timing of the phase transition ($r_s = 0.77$), with later transitions associated with higher annual totals. In contrast, no clear relationship is observed between annual precipitation and the characteristics of the core monsoon phase. Within the pre-onset phase, precipitation amount is highly variable (285 ± 109 mm, n = 7) and closely related to phase duration ($r_s = 0.77$). For the core monsoon phase, total precipitation is less variable (1242 ± 70 mm, n = 7) and only correlated with hourly intensity ($r_s = 0.79$). In addition, a strong negative relationship is observed between the core phase duration and accumulation rate ($r_s = -1.00$), indicating a compensation between these two variables.

https://doi.org/10.5194/egusphere-2026-5233
Preprint. Discussion started: 14 September 2026

458 The timing of the different seasonal transitions further constrains phase characteristics. The duration of the pre-onset phase is controlled by the timing of the first rainfall events (r_s = -0.85), whereas the duration of the core monsoon phase is governed by the timing of the phase transition (r_s = -0.85). The monsoon retreat date, although relatively stable, is associated with variations in mean hourly intensity during the core monsoon phase (0.78).

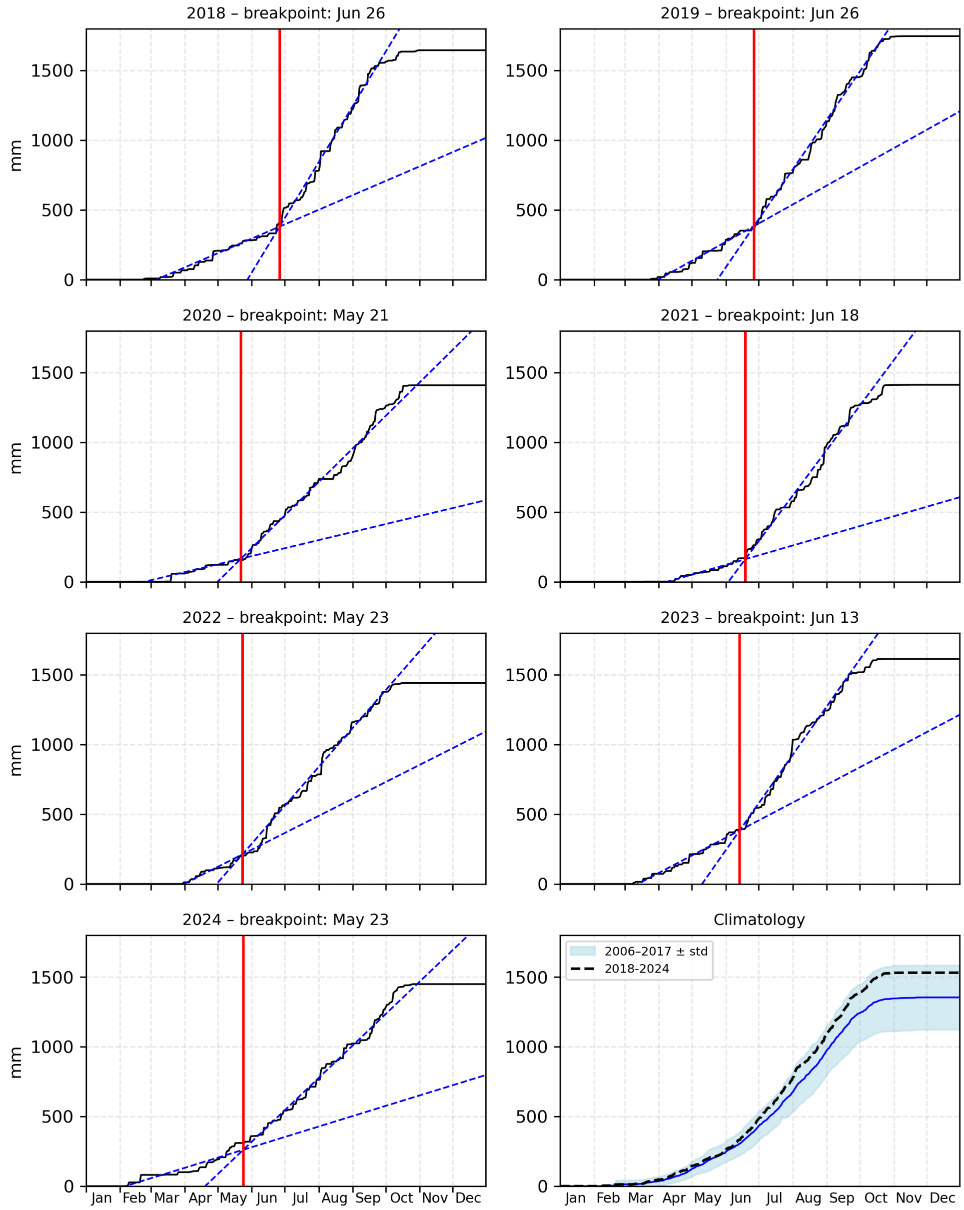

462

https://doi.org/10.5194/egusphere-2026-5233
Preprint. Discussion started: 14 September 2026

Figure 8: Annual cumulative daily precipitation at the inland site between 2018 and 2024. Blue dotted lines indicate the average linear trends associated with the two monsoon phases. Red vertical lines mark the breakpoints, defined as the intersection of the two linear regressions.

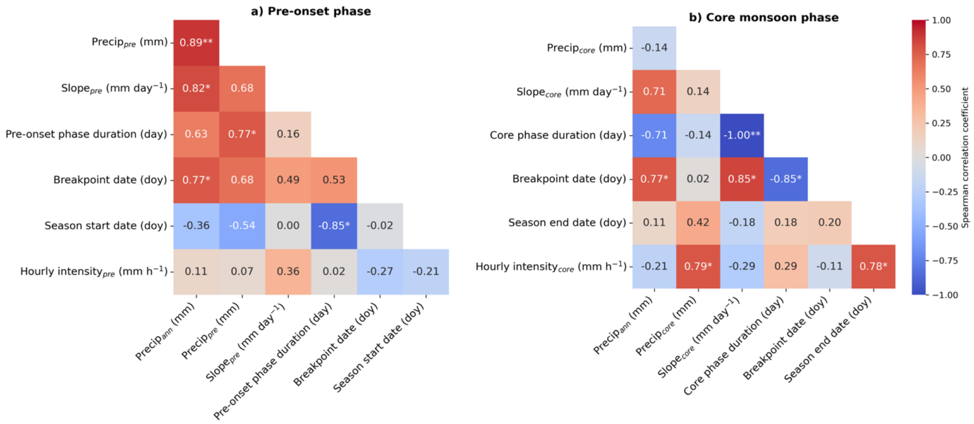

Figure 9: Spearman rank correlation matrices showing relationships among annual characteristics of the (a) pre-onset and (b) core monsoon phases. Variables include annual and phase precipitation totals, mean daily rainfall accumulation rate (i.e. the slopes in Fig. 8), phase duration, key timing dates (doy: day of year), and mean hourly rainfall intensity. Spearman correlation coefficients are shown, with statistical significance indicated by asterisks (* $p < 0.05$, ** $p < 0.01$; $n = 7$ years).

3.4.2 Phase-dependent meteorological and isotopic characteristics

The proportion of non-sampled rainfall varies between 1 and 9% annually and primarily affects the pre-onset phase, representing between 2% and 85% of its total precipitation, compared with 0–6% for the core monsoon phase. The pre-onset phase is mainly associated with rainfall events from clusters C1 and C2, whereas the core monsoon phase is dominated by clusters C2 and C3, with only sporadic occurrences of C1, mostly toward the end of the season. The vast majority of C3 rainfall occurs during the core monsoon phase.

The two phases exhibit distinct isotopic signatures. The pre-onset phase is characterized by more enriched $\delta^{18}O$ values, ranging from −1.5 to −3.6 ‰ (−2.41 ± 0.86 ‰), whereas the core monsoon phase shows more depleted values, ranging from −4.3 to −5.8 ‰ (−4.94 ± 0.45 ‰). In contrast, d-excess exhibits substantial interannual variability but does not differ significantly between the two phases (11.6 ± 1.6 ‰ for the pre-onset phase and 11.9 ± 1.0 ‰ for the core monsoon phase). Variations in ^{17}O-excess are more limited, with slightly higher values during the core monsoon phase (21 ± 2 per meg) compared to the pre-onset phase (16 ± 3 per meg).

Relationships between isotopic composition and meteorological variables were explored at the annual scale using the non-parametric Spearman rank correlation (Figure 10). Due to the potential bias introduced by non-sampled rainfall, the pre-onset phase was not considered in this analysis. Annual precipitation-weighted mean $\delta^{18}O$ shows strong negative correlations with both mean hourly precipitation intensity during the core monsoon phase (r_s =

https://doi.org/10.5194/egusphere-2026-5233
Preprint. Discussion started: 14 September 2026

−0.89, $p < 0.01$), and core monsoon phase precipitation amount (r_s = -0.82, $p < 0.05$). The timing of the monsoon retreat is strongly correlated with core monsoon phase precipitation-weighted mean $\delta^{18}O$ (r_s = -0.84, $p < 0.05$), and more weakly with annual precipitation-weighted mean $\delta^{18}O$ (r_s = -0.76, $p < 0.05$). No other significant relationships are identified for $\delta^{18}O$, and none for d-excess and ^{17}O-excess.

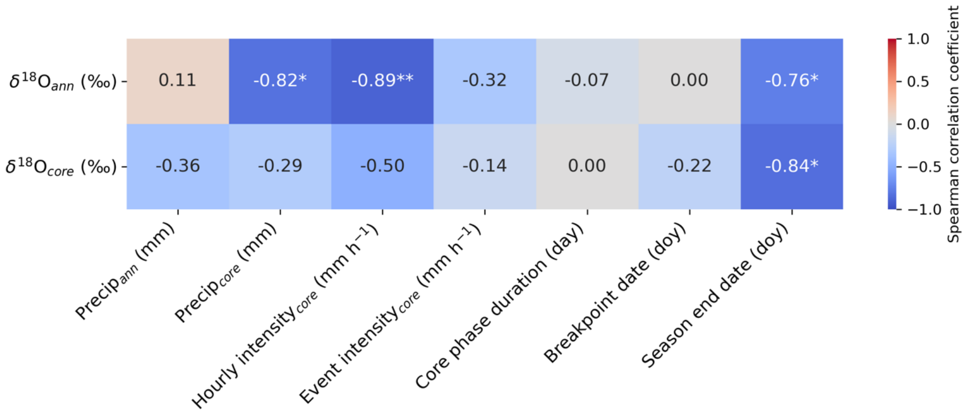

Figure 10: Spearman rank correlations between annual precipitation-weighted $\delta^{18}O$ values and annual climatic variables (n = 7 years). Correlation coefficients are shown together with their statistical significance (* $p < 0.05$, ** $p < 0.01$).

4. Discussion

4.1 Microphysical and convective influences on precipitation isotopes

In this section, "microphysical processes" refers to the cloud and precipitation processes that modify the isotopic composition of rainfall, including condensation, evaporation of falling raindrops, and phase changes within precipitating systems. The interpretation is based on the different combinations of $\delta^{18}O$, ^{17}O-excess and d-excess values observed in the three isotopic clusters identified at the inland site, together with the associated rainfall and meteorological characteristics (Figures 5 and 6). These isotopic signatures are interpreted as reflecting varying contributions of equilibrium and kinetic isotope fractionation processes, which are discussed below.

In cluster C1, the combination of enriched $\delta^{18}O$ and low d-excess and ^{17}O-excess, and their correlation with RH, is consistent with sub-cloud evaporation, where falling raindrops partially evaporate in relatively dry air below the cloud base. This process is typically associated with isolated convective cells developing in environments characterized by low relative humidity (Landais et al., 2010). This interpretation is supported by the meteorological characteristics associated with this cluster: drier and warmer atmospheric conditions and higher outgoing longwave radiation (OLR) are consistent with less extensive and less organized convective activity. In addition, short-duration but relatively intense rainfall events are revealed by the 5-min event analysis, although hourly rainfall intensities remain moderate (Figure 6). This suggests locally driven convective bursts in a dry environment.

https://doi.org/10.5194/egusphere-2026-5233
Preprint. Discussion started: 14 September 2026

In contrast, cluster C2 and C3, which together account for approximately 85% of total rainfall, are characterized by longer event durations than for cluster C1, consistent with more organized convective systems. They differ from each other in their isotopic and meteorological characteristics. Cluster C3 exhibits more depleted δ^{18}O values, lower hourly rainfall intensities, greater daily rainfall persistence, and a larger fraction of weak precipitation events compared to C2. In addition, it is associated with higher relative humidity and lower OLR values, suggesting more extensive cloud cover and a greater degree of convective organization. Such characteristics are consistent with a larger contribution from the stratiform regions of MCSs, which are typically associated with weaker but more persistent rainfall, and more depleted δ^{18}O values (Aggarwal et al., 2016; Risi et al., 2023). Taken together, these observations are consistent with C3 being associated with more mature and organized convective systems, abnd a potentially larger contribution from the stratiform regions of MCSs than in cluster C2.

Interestingly, cluster C2 and C3 together display a trend in which the depleted δ^{18}O values of C3 are associated with lower ^{17}O-excess and d-excess (Figure 5). This contrasts with the isotopic signature generally associated with sub-cloud evaporation, for which δ^{18}O and excess parameter tend to be negatively correlated. The processes responsible for the decrease in ^{17}O-excess associated with C3 remain uncertain. The low values of ^{17}O-excess and d-excess observed in this cluster suggest that kinetic fractionation processes may influence the isotopic signature of precipitation within organized convective systems. The different processes involving kinetic fractionation that may operate within the stratiform regions of tropical MCSs are described in (Risi et al., 2023). They mainly involve rain evaporation and subsequent rain-vapor diffusive exchanges within downdraft regions of stratiform precipitation areas. Such internal atmospheric vapor recycling within the convective structure has been proposed as a mechanism that can contribute to strong δ^{18}O depletion and to modify the kinetic signature expressed by excess parameters (d-excess and probably also ^{17}O-excess). In addition, deep convective cells often attain the upper troposphere and integrate depleted vapor from the free atmosphere. However, these processes, either moisture recycling or upper troposphere contribution, are generally expected to increase excess parameters in atmospheric vapor, as observed in d-excess measurements of surface vapor within a Sahelian climatic context (Tremoy et al., 2014), and in ^{17}O-excess observations in Singapore (Zhang et al., 2024). In contrast, we observe lower mean ^{17}O-excess and d-excess associated with depleted δ^{18}O during the rainfall classified as C3.

To our knowledge, the only cases in which δ^{18}O depletion accompanied by ^{17}O-excess decrease was observed come from polar studies (Surma et al., 2021 and references therein), where kinetic effects associated with ice supersaturation lead to decreased ^{17}O-excess values for strongly depleted values of δ^{18}O (δ^{18}O < -40 ‰). Although the isotopic range differs markedly from polar observations, the MCSs in the WAM involve extensive ice-phase processes (Houze, 2004; Xu and Zipser, 2012). Combined with intense vertical velocities as observed by (Heymsfield et al., 2010), this could favor kinetic fractionation during vapor deposition onto ice. This mechanism could therefore contribute to lowering ^{17}O-excess values. Although such an effect has not yet been documented in tropical precipitation, our data suggest that this process may deserve further investigations in deep tropical systems. The available observations do not allow for distinguishing between the two types of kinetic processes responsible for the observed ^{17}O-excess decrease: internal vapor recycling, and supersaturation effects with respect to ice. Dedicated vapor isotope measurements together with isotope-enabled simulations of MCSs would be required to assess their respective contributions. Additional moisture transported within the African Easterly Jet or Tropical Easterly Jet may also contribute to the isotopic composition of mature MCSs (Niang et al. 2020). However, its

https://doi.org/10.5194/egusphere-2026-5233
Preprint. Discussion started: 14 September 2026

contribution cannot be constraint from our HYSPLIT analysis, which does not resolve entrainment and detrainment processes occurring within deep convective systems. Isotope-enabled convection-resolving modelling would therefore be required to assess its potential role.

Overall, the isotopic clustering suggests distinct precipitation regimes associated with different convective organizations, ranging from isolated short-lived convective cells, where rainfall is potentially affected by sub-cloud evaporation (C1), to progressively more organized convective systems with an increasing contribution from precipitation associated with large-scale monsoon circulation. As observed in previous studies (Sun et al., 2024; Zhang et al., 2024), the results therefore support the view that precipitation isotopes in the WAM are strongly influenced by convective organization.

4.2 Continental moisture contribution: a weak but coherent signature

Although microphysical processes appear to have an important influence on the isotopic clustering, the excess parameters may also retain information on moisture source conditions. This has been demonstrated for oceanic moisture source using d-excess since the pioneer study of (Gat and Carmi, 1970), as well as more recently through the evidence of a relationship between ^{17}O-excess variability in precipitation and changes in evaporation conditions at oceanic moisture source (Uechi and Uemura, 2019).

On the other hand, the additional contribution of moisture sources originating from continental evapotranspiration has been increasingly recognized as an important component of the WAM (Nicholson, 2013; Yu et al., 2017). Isotopic tracers also have the potential to reveal such processes as continental moisture recycling has been shown to increase d-excess in atmospheric vapor and precipitation (Aemisegger et al., 2014; Delattre et al., 2015; Natali et al., 2022; Taupin et al., 2000; Vallet-Coulomb et al., 2008; Xia and Winnick, 2021). However, evidence for a similar influence on ^{17}O-excess remains scarce. Atmospheric moisture produced by continental evaporation is characterized by an isotopic signature depleted in δ^{18}O and enriched in d-excess, while transpiration transfers soil water to the atmosphere with little fractionation, therefore producing a vapor enriched in δ^{18}O and unmodified in d-excess compared to regional atmospheric moisture. Overall, and similar to what was observed for d-excess, the integration of evapotranspiration to regional atmospheric moisture, and thereafter to precipitation formation is expected to carry higher ^{17}O-excess signatures (Voigt et al., 2026; Xia et al., 2023).

The HYSPLIT analysis provides a regional-scale description of the dominant transport pathways and moisture uptake represented by the meteorological reanalysis that feed the lower troposphere prior to convective development, although the detailed three-dimensional moisture budget within convective systems cannot be solved within this framework. In our case, the back-trajectory analysis indicates that for both stations, oceanic moisture sources are similarly spread along a mean air-mass trajectory extending from approximately 20°S to the Gulf of Guinea coast. Therefore, considering the homogeneity of their respective oceanic moisture source, we don't expect that oceanic moisture source conditions could be a major driver of observed variations. On the other hand, an additional regional surface moisture uptake is identified for the inland site over continental areas (Figure 2). Notably, this continental moisture source encompasses the region of Lake Volta (Ghana), whose huge open-water

https://doi.org/10.5194/egusphere-2026-5233
Preprint. Discussion started: 14 September 2026

surface (~8500 km², *i.e.* the largest artificial lake in the world) may represent an important regional source of atmospheric moisture.

The paired observations from the coastal and inland sites, located along the same large-scale oceanic monsoon flow, provide a good opportunity to examine how isotopic signals, and specifically the ^{17}O-excess, evolve under a continental influence, with the coastal station serving as a benchmark representing precipitation influenced by oceanic moisture sources. Among the three isotopic clusters observed inland, only C1 and C2 are also observed at the coastal station. C1 exhibits similar isotopic characteristics at both sites, whereas C3, characterized by strongly depleted δ^{18}O, is absent at the coast, likely reflecting the reduced contribution from MCSs at the coastal site, where convection tends to be more localized and of smaller spatial extent (Xu and Zipser, 2012). The comparison therefore provides the clearest basis for examining the inland shift in the isotopic composition of C2, which exhibits higher ^{17}O-excess values inland and, to a lesser extent, higher d-excess, than its coastal counterpart, despite comparable δ^{18}O values. Because ^{17}O-excess is largely insensitive to Rayleigh processes and primarily responds to kinetic fractionation processes, these higher inland values are consistent with an additional contribution of continental moisture to precipitation. Overall, the comparison between the two sites reveals a weak but coherent isotopic signature of continental moisture recycling, consistent with the regional transport pathways identified by HYSPLIT.

4.3 Seasonal isotopic changes associated with monsoon convective organization

The cumulative precipitation analysis allowed us to identify a transition between a pre-onset and a core monsoon phases, occurring around the beginning of June (Figure 8). This transition is broadly with the onset stage described at the regional scale by (Sultan and Janicot, 2003), who identified a comparable abrupt increase rainfall accumulation around June 24th (+/- 8 days) over the 1968-1990 period, although the transition is defined here using a precipitation-based criterion rather than circulation-based metrics. Thereafter, the core monsoon phase corresponds to well-established monsoon conditions that persists until a relatively abrupt withdrawal in October, consistent with previous descriptions (Le Barbé et al., 2002; Sultan and Janicot, 2003).

Isotopically, the seasonal transition is also a transition in the relative occurrence of the isotopic rainfall regimes. The pre-onset phase is dominated by rainfall events belonging to cluster C1, characterized by short-lived convective bursts, while the contribution of C2 progressively increases (Figure 7). In contrast, the core monsoon phase is characterized by the prevalence of clusters C2 and C3. Cluster C2 dominates until approximately mid-August, when it is progressively replaced by cluster C3, coinciding with the period when the rain belt reaches its northernmost position and the monsoon system becomes fully established over West Africa. Interestingly, this transition occurs despite only limited changes in local rainfall amounts. This observation suggests that seasonal isotopic variability is more closely linked to changes in convective organization than with local rainfall amounts, with a shift toward larger and more mature convective systems, potentially involving a greater contribution from their stratiform regions. Such a seasonal picture, consistent with the meteorological and isotopic characteristics of cluster C3 described above, underlines that sub-seasonal isotopic variability is closely associated with the seasonal progression of the West African monsoon system, through its influence on convective organization.

https://doi.org/10.5194/egusphere-2026-5233
Preprint. Discussion started: 14 September 2026

4.4 Interannual isotopic variability beyond a simple amount effect

A key result of the two-phase analysis is that annual rainfall amount and annual precipitation-weighted isotopic composition are primarily driven by different components of the monsoon season. Annual rainfall totals are primarily modulated by the contribution of the pre-onset phase, whereas annual isotopic composition is mainly linked to rainfall occurring during the core monsoon phase, as indicated by its relationships with core-phase rainfall amount, hourly rainfall intensity, and monsoon retreat date (Figures 9 and 10). These contrasting behavior suggests that annual amount-weighted $\delta^{18}O$ mean is more sensitive to the amount and characteristics of rainfall during the mature monsoon phase than to the annual hydrological budget itself. Conversely, although accounting for a limited fraction of annual rainfall, the pre-onset phase remains hydrologically important because it largely contributes annual rainfall anomalies and conditions the development of vegetation and land-surface feedbacks.

The substantial interannual variability in precipitation-weighted $\delta^{18}O$ (from −4.3 to −5.8 ‰ for the core monsoon phase) probably reflect the combined influences of convective dynamics, cloud microphysics and continental moisture recycling. In particular, rainfall events associated with the more organized precipitation systems represented by cluster C3 are associated with more depleted $\delta^{18}O$ values, suggesting a potential contribution of these rainfall regimes to isotopic depletion. However, the relative contribution of these processes cannot be quantitatively separated from observations alone, and a combined isotope-enabled modelling approach would be required to further disentangle the respective roles of convective dynamics, cloud microphysics and continental moisture recycling. Such an approach would also help assess how future changes in monsoon organization may be recorded in precipitation isotopes. For instance, a long-term increase in the persistence of mature monsoon conditions and organized convective systems could potentially lead to more depleted $\delta^{18}O$ values, potentially accompanied by modifications of ^{17}O-excess and d-excess.

The interpretation of precipitation isotopes in paleoclimatic and paleohydrological archives often relies on the assumption that lower $\delta^{18}O$ values reflect wetter climatic conditions through the amount effect, first introduced by (Dansgaard, 1964). However, although limited to seven years and covering relatively wet conditions, the present dataset indicates that the monthly-scale amount effect is restricted to low-precipitation conditions, and largely driven by enhanced sub-cloud evaporation. During the core monsoon season, however, annual $\delta^{18}O$ is significantly related to core-phase rainfall amount and hourly rainfall intensity, while no significant relationship is observed with total annual rainfall amount.

Previous studies have shown that precipitation $\delta^{18}O$ in tropical regions is influenced by several processes acting at different spatial and temporal scales. Some studies emphasize the dominant role of upstream rainout history over local rainfall amount (Kurita et al., 2009; Nlend et al., 2020; Zhang et al., 2024), whereas others relate isotopic depletion to convective intensity using proxies such as outgoing longwave radiation (Yu et al., 2024). At the cloud scale, isotopic depletion has been attributed to processes occurring within MCSs, including moisture recycling in unsaturated downdrafts (Risi et al., 2023) or the increasing contribution of stratiform precipitation (Aggarwal et al., 2016; Munksgaard et al., 2019). Rather than being contradictory, these mechanisms likely describe complementary aspects of convective organization, since larger and longer-lived convective systems simultaneously experience stronger rainout, more extensive stratiform regions, and more complex internal moisture recycling.

Together, these results indicate that interannual variations in precipitation $\delta^{18}O$ at Nalohou are not simply related to the annual rainfall budget, but are more closely associated with the amount and characteristics of rainfall during the mature monsoon phase.

5- Conclusion

This study shows that precipitation isotopes in the Sudanian WAM, and particularly ^{17}O-excess, are strongly driven by convective organization and associated cloud microphysical processes. In addition, a weak but coherent signature of continental moisture recycling is detected at the inland station, through higher ^{17}O-excess and d-excess values than at the coastal station. The contribution of continental moisture is consistent with the moisture source analysis, which identifies a major continental source region encompassing the Lake Volta area (8500 km^2) in Ghana, which may represent an important regional source of evaporation. Although secondary compared to the convective controls, this isotopic signal indicates that excess parameters may retain information on land–atmosphere moisture exchanges.

A particularly original result concerns the isotopic signature of the most mature convective systems (cluster C3), characterized by strongly depleted $\delta^{18}O$ values associated with simultaneous decreases in both d-excess and ^{17}O-excess. This result suggests the influence of specific kinetic fractionation processes that may operate within stratiform regions of MCSs, potentially associated with vapor recycling within stratiform downdrafts or supersaturation effects during ice-phase formation in deep convective clouds. Although these processes cannot be individually resolved with the present dataset, this result highlights the potential of triple oxygen isotopes to provide additional constraints for investigating atmospheric processes and cloud microphysics in the WAM.

At the interannual scale, we show the importance of the pre-onset phase, which, despite its relatively limited contribution to annual totals, modulates annual rainfall variability and plays a key role in regional hydrological functioning by replenishing soil moisture and enabling the onset of vegetation growth. However, interannual variations in $\delta^{18}O$ are primarily associated with the core monsoon phase, during which precipitation isotope composition primarily reflects the development and organization of MCSs, rather than the annual hydrological budget.

The sampling strategy adopted in this study provides a compromise between temporal resolution and the logistical constraints inherent to long-term monitoring in remote regions of West Africa. Although samples do not systematically correspond to individual precipitation events, the relatively high sampling frequency captures rainfall variability at a temporal resolution sufficient to identify intra-seasonal transitions in the main isotopic regimes and their seasonal evolution. In addition, the size of the dataset provides sufficient statistical power to identify coherent isotopic patterns despite the relatively limited variability of ^{17}O-excess compared with the analytical uncertainty. A fully event-based sampling strategy, combined with concurrent vapor isotope measurements, would further improve the characterization of cloud microphysical processes, but such observations

https://doi.org/10.5194/egusphere-2026-5233
Preprint. Discussion started: 14 September 2026

remain particularly demanding in terms of field logistics and sustained observational infrastructure. In this context, the present 7-year record constitutes a unique dataset for the region.

The continuation of this long-term monitoring within the long-term AMMA-Catch observatory framework will provide an increasingly valuable basis for evaluating isotope-enabled climate models and, over longer time scales, for assessing climatic trends in the WAM, and refining the interpretation of tropical paleoclimate archives. In particular, the combined interpretation of $\delta^{18}O$, d-excess and ^{17}O-excess provides a valuable benchmark for testing model representations of convective organization, cloud microphysics and moisture recycling within the WAM.

Appendix A

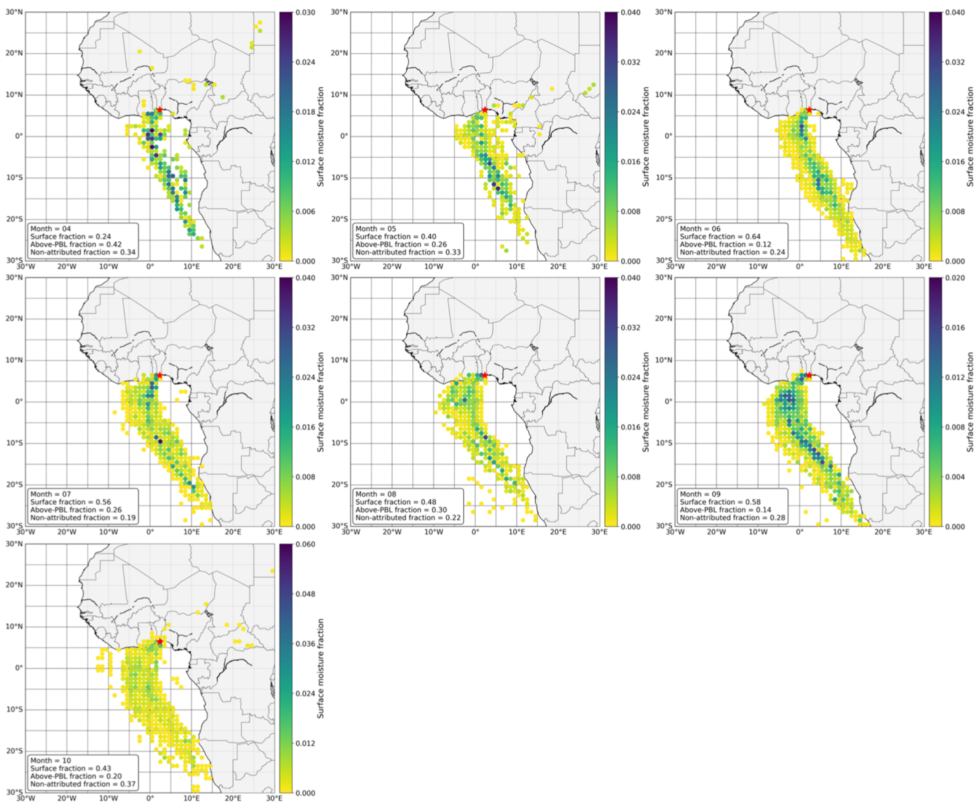

Figure A1: Monthly moisture source regions derived from back-trajectory analysis, expressed as a fraction of total precipitation at the coastal site.

https://doi.org/10.5194/egusphere-2026-5233
Preprint. Discussion started: 14 September 2026

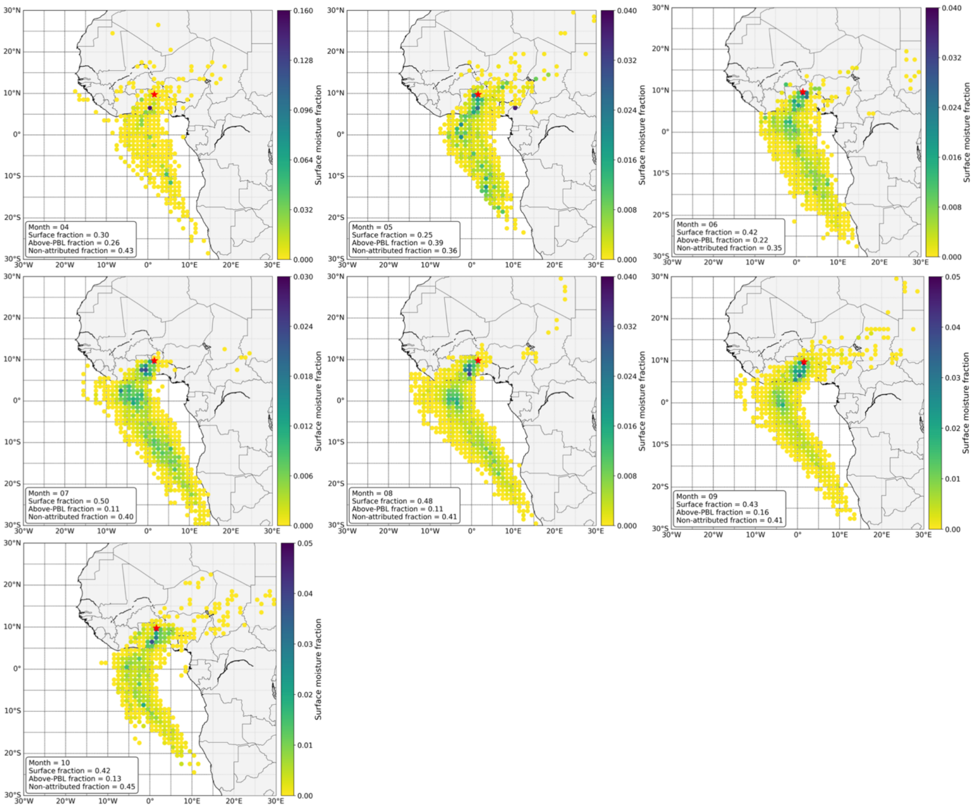

Figure A2: Monthly moisture source regions derived from back-trajectory analysis, expressed as a fraction of total precipitation at the inland site.

https://doi.org/10.5194/egusphere-2026-5233
Preprint. Discussion started: 14 September 2026

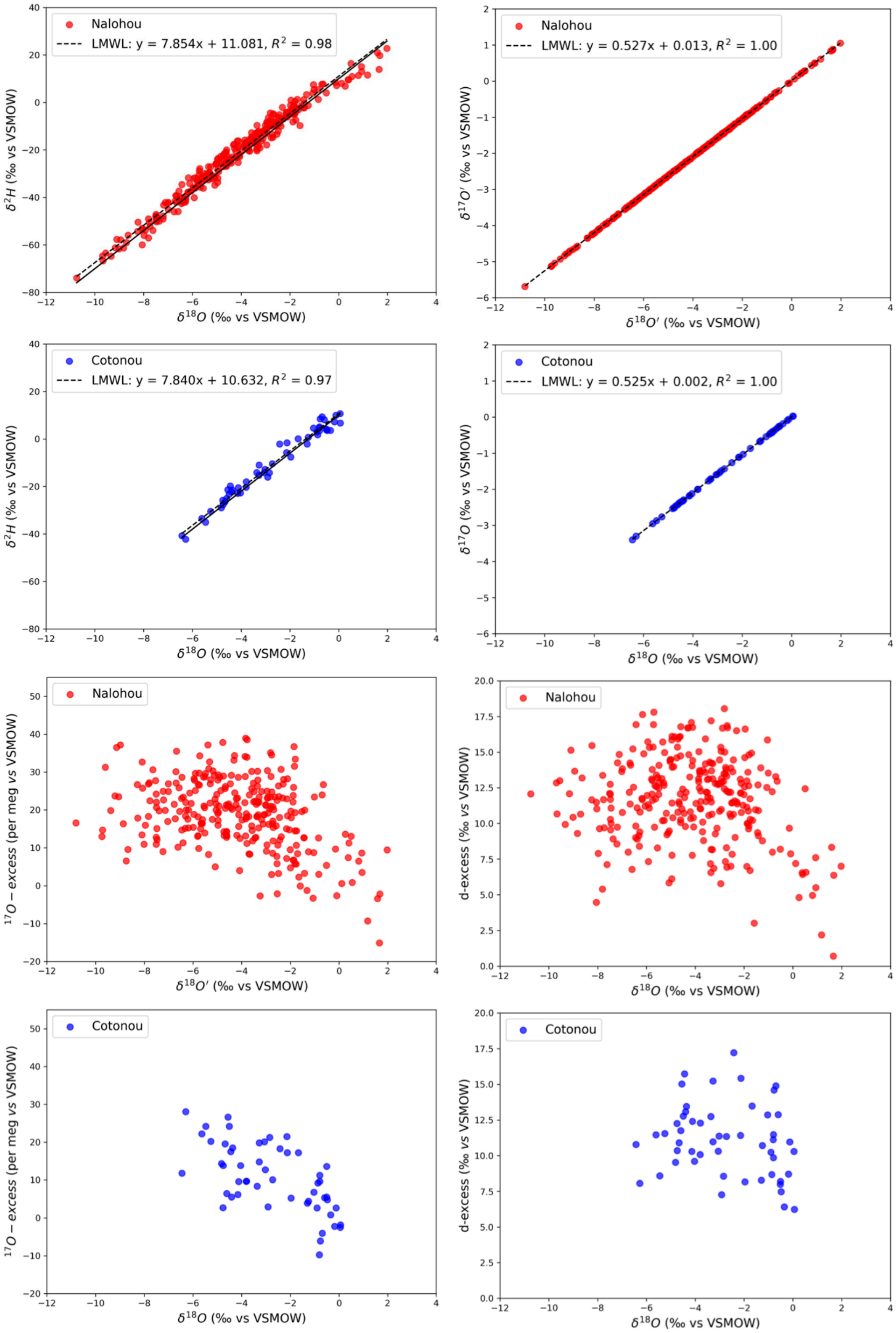

https://doi.org/10.5194/egusphere-2026-5233
Preprint. Discussion started: 14 September 2026

Figure A3: Plots of δ^2H vs $\delta^{18}O$, $\delta^{17}O'$ vs $\delta^{18}O'$ for the inland (a, b) and coastal (c, d) stations, with the corresponding Local Meteoric water lines (LMWL) as dashed lines, and the global meteoric water line (black line in a and c). Plots of ^{17}O-excess vs $\delta^{18}O'$ and d-excess vs $\delta^{18}O$ for the inland (e, f) and coastal (g, h) stations.

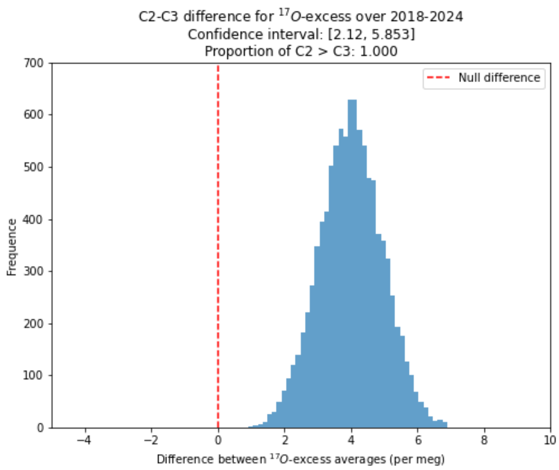

Figure A4: Monte Carlo distribution of the difference in mean ^{17}O-excess between clusters C2 and C3 at the inland site. The histogram shows the distribution of differences in cluster-mean ^{17}O-excess (C2 − C3) obtained from 10,000 Monte Carlo simulations, accounting for analytical uncertainty (±7 per meg, assumed Gaussian and independent). The vertical dashed line indicates zero difference.

Data availability

Open-access 5-minute rainfall and meteorological datasets are available on the AMMA-CATCH data portal (doi: 0.17178/AMMA-CATCH.CL.Rain_Od for Nalohou 2 and Nalohou 3 rain gauges, doi :10.17178/AMMA-CATCH.AE.H2OFlux_Odc for meteorological variables at the Nalohou flux station). Rainfall isotopes datasets will be made available on the AMMA-CATCH data portal.

Author contribution: CVC designed the study, coordinated sample collection and transport with CP, performed the statistical and HYSPLIT analyses with contributions from DCE and AZ. CVC developed the interpretation of the isotopic and meteorological results with contributions from CP, DCE, AAL and VK and CV. AAL and VK supervised sample collection at the Abomey-Calavi station, whereas CP and RH supervised sample collection at Nalohou. TO, SA, and VG collected samples. CVC and DAY performed isotopic measurements at CEREGE. AAA led the ANR project that supported the study. CVC prepared the manuscript with contributions from all co-authors. (AAL: Abdoukarim Alassane and AAA: Anne Alexandre)

Competing interests: The authors declare that they have no conflict of interest.

Statement on inclusion in global research: This study builds on more than two decades of long-term environmental observations conducted through the AMMA-Catch observatory in partnership with researchers and institutions in Benin and France, with support from IRD. The coastal station was established in collaboration with researchers at the University of Abomey-Calavi and is now being continued within the framework of the REZOC International Mixed Laboratory. Results from this work are intended to support the continued development of regional observational capacities and the use of isotopic tracers in water resources research conducted by Beninese teams.

Acknowlegments: The authors are particularly grateful to the AMMA-CATCH observatory team, especially Mr Moussa Dawerema who took care of rainfall sampling at Nalohou, Dr G. Panthou and M. Soumaïla who made available precipitation datasets, and Mrs O. Mamadou and M. JM Cohard who cured meteorological datasets.

Financial support: This work was funded by the French Research Agency (ANR) through the HUMI-17 project (ANR-17-CE01-0002-01), by the French INSU-CNRS national research program EC2CO (Continental and Coastal Ecosphere) and by the IRD (Research Institute for development).

References

Aemisegger, F., Pfahl, S., Sodemann, H., Lehner, I., Seneviratne, S.I., Wernli, H., 2014. Deuterium excess as a proxy for continental moisture recycling and plant transpiration. Atmospheric Chemistry and Physics 14, 4029–4054. https://doi.org/10.5194/acp-14-4029-2014

Aggarwal, P.K., Romatschke, U., Araguas-Araguas, L., Belachew, D., Longstaffe, F.J., Berg, P., Schumacher, C., Funk, A., 2016. Proportions of convective and stratiform precipitation revealed in water isotope ratios. Nat. Geosci. 9, 624-+. https://doi.org/10.1038/NGEO2739

Aïzansi, A.N., Ogunjobi, K.O., Ogou, F.K., 2024. Monthly rainfall prediction using artificial neural network (case study: Republic of Benin). Environmental Data Science 3, e11. https://doi.org/10.1017/eds.2024.10

Alexandre, A., Outrequin, C., Vallet-Coulomb, C., Peugeot, C., Grippa, M., Aleman, J., Voigt, C., Landais, A., Mougin, E., Ndiaye, O., Sonzogni, C., Yang, D.A., Mazur, J., Couapel, M., Ogée, J., Ouani, T., Afouda, S., Wubda, M., Soumaguel, N., Houngnon, A., Tagesson, T., Fensholt, R., 2025. What Does the Triple Isotopic Composition of Oxygen in Precipitation, Groundwater, Soil Water, Plant Water, and Phytoliths Reveal About Current and Past Hydrological Cycles? JGR Biogeosciences 130, e2024JG008615. https://doi.org/10.1029/2024JG008615

Aron, P.G., Levin, N.E., Beverly, E.J., Huth, T.E., Passey, B.H., Pelletier, E.M., Poulsen, C.J., Winkelstern, I.Z., Yarian, D.A., 2020. Triple oxygen isotopes in the water cycle. Chemical Geology 120026. https://doi.org/10.1016/j.chemgeo.2020.120026

Bailey, A., Noone, D., Dee, S., Nusbaumer, J., Conroy, J., Stevenson, S., Atwood, A., 2025. Toward a process-oriented understanding of water in the climate system: recent insights from stable isotopes. Environ. Res.: Climate 4, 012002. https://doi.org/10.1088/2752-5295/ada17b

Biasutti, M., 2019. Rainfall trends in the African Sahel: Characteristics, processes, and causes. WIREs Climate Change 10, e591. https://doi.org/10.1002/wcc.591

Cai, Z., Tian, L., Bowen, G.J., 2018. Spatial-seasonal patterns reveal large-scale atmospheric controls on Asian Monsoon precipitation water isotope ratios. Earth and Planetary Science Letters 503, 158–169. https://doi.org/10.1016/j.epsl.2018.09.028

Chagnaud, G., Blanchet, J., Evin, G., Hingray, B., Lebel, T., Panthou, G., Vischel, T., 2024. How fast is the frequency of precipitation extremes doubling in global land regions? Environ. Res. Commun. 6, 121010. https://doi.org/10.1088/2515-7620/ad9f12

Chagnaud, G., Panthou, G., Vischel, T., Lebel, T., 2022. A synthetic view of rainfall intensification in the West African Sahel. Environ. Res. Lett. 17, 044005. https://doi.org/10.1088/1748-9326/ac4a9c

Dansgaard, W., 1964. Stable isotopes in precipitation. Tellus 16, 436–468.

Delattre, H., Vallet-Coulomb, C., Sonzogni, C., 2015. Deuterium excess in the atmospheric water vapour of a Mediterranean coastal wetland: regional vs. local signatures. Atmos. Chem. Phys. 15, 10167–10181. https://doi.org/10.5194/acp-15-10167-2015

https://doi.org/10.5194/egusphere-2026-5233
Preprint. Discussion started: 14 September 2026

Fiorella, R.P., Siler, N., Nusbaumer, J., Noone, D.C., 2021. Enhancing Understanding of the Hydrological Cycle via Pairing of Process-Oriented and Isotope Ratio Tracers. J Adv Model Earth Syst 13, e2021MS002648. https://doi.org/10.1029/2021MS002648

Galle, S., Grippa, M., Peugeot, C., Moussa, I.B., Cappelaere, B., Demarty, J., Mougin, E., Panthou, G., Adjomayi, P., Agbossou, E.K., Ba, A., Boucher, M., Cohard, J.-M., Descloitres, M., Descroix, L., Diawara, M., Dossou, M., Favreau, G., Gangneron, F., Gosset, M., Hector, B., Hiernaux, P., Issoufou, B.-A., Kergoat, L., Lawin, E., Lebel, T., Legchenko, A., Abdou, M.M., Malam-Issa, O., Mamadou, O., Nazoumou, Y., Pellarin, T., Quantin, G., Sambou, B., Seghieri, J., Seguis, L., Vandervaere, J.-P., Vischel, T., Vouillamoz, J.-M., Zannou, A., Afouda, S., Alhassane, A., Arjounin, M., Barral, H., Biron, R., Cazenave, F., Chaffard, V., Chazarin, J.-P., Guyard, H., Kone, A., Mainassara, I., Mamane, A., Oi, M., Ouani, T., Soumaguel, N., Wubda, M., Ago, E.E., Alle, I.C., Allies, A., Arpin-Pont, F., Awessou, B., Charvet, G., Casse, C., Dardel, C., Depeyre, A., Diallo, F.B., Do, T., Fatras, C., Frappart, F., Gal, L., Gascon, T., Gibon, F., Guiro, I., Ingatan, A., Kempf, J., Kotchoni, D.O., Lawson, F.M.A., Leauthaud, C., Louvet, S., Mason, E., Nguyen, C.C., Perrimond, B., Pierre, C., Richard, A., Robert, E., Roman-Cascon, C., Velluet, C., Wilcox, C., 2018. AMMA-CATCH, a Critical Zone Observatory in West Africa Monitoring a Region in Transition. Vadose Zone J. 17, 180062. https://doi.org/10.2136/vzj2018.03.0062

Gat, J.R., Carmi, I., 1970. Evolution of the isotopic composition of atmospheric waters in the Mediterranean Sea area. J. Geophys. Res. 75, 3039–3048. https://doi.org/10.1029/JC075i015p03039

Giannini, A., Saravanan, R., Chang, P., 2003. Oceanic Forcing of Sahel Rainfall on Interannual to Interdecadal Time Scales. Science 302, 1027–1030. https://doi.org/10.1126/science.1089357

Giorgi, F., 2002. Variability and trends of sub-continental scale surface climate in the twentieth century. Part I: observations. Climate Dynamics 18, 675–691. https://doi.org/10.1007/s00382-001-0204-x

Gröning, M., Lutz, H.O., Roller-Lutz, Z., Kralik, M., Gourcy, L., Pöltenstein, L., 2012. A simple rain collector preventing water re-evaporation dedicated for δ18O and δ2H analysis of cumulative precipitation samples. Journal of Hydrology 448–449, 195–200. https://doi.org/10.1016/j.jhydrol.2012.04.041

Guan, H., Zhang, X., Skrzypek, G., Sun, Z., Xu, X., 2013. Deuterium excess variations of rainfall events in a coastal area of South Australia and its relationship with synoptic weather systems and atmospheric moisture sources. JGR Atmospheres 118, 1123–1138. https://doi.org/10.1002/jgrd.50137

Hassenruck-Gudipati, H.J., Andermann, C., Dee, S., Brunello, C.F., Baidya, K.P., Sachse, D., Meyer, H., Hovius, N., 2023. Moisture Sources and Pathways Determine Stable Isotope Signature of Himalayan Waters in Nepal. AGU Advances 4, e2022AV000735. https://doi.org/10.1029/2022AV000735

He, S., Jackisch, D., Samanta, D., Yi, P.K.Y., Liu, G., Wang, X., Goodkin, N.F., 2021. Understanding Tropical Convection Through Triple Oxygen Isotopes of Precipitation From the Maritime Continent. J. Geophys. Res.-Atmos. 126, e2020JD033418. https://doi.org/10.1029/2020JD033418

Hersbach, H., Bell, B., Berrisford, P., Biavati, G., Horanyi, A., Muñoz Sabater, J., Nicolas, J., Peubey, C., Radu, R., Rozum, I., Schepers, D., Simmons, A., Soci, C., Dee, D., Thepaut, J.-N., 2023. ERA5 hourly data on single levels from 1940 to present. https://doi.org/10.24381/CDS.ADBB2D47

Heymsfield, G.M., Tian, L., Heymsfield, A.J., Li, L., Guimond, S., 2010. Characteristics of Deep Tropical and Subtropical Convection from Nadir-Viewing High-Altitude Airborne Doppler Radar. Journal of the Atmospheric Sciences 67, 285–308. https://doi.org/10.1175/2009JAS3132.1

Houze, R.A., 2004. Mesoscale convective systems. Reviews of Geophysics 42, 2004RG000150. https://doi.org/10.1029/2004RG000150

Hulme, M., 1992. Rainfall changes in Africa: 1931-1960 to 1961-1990. International Journal of Climatology 12, 685–699.

Jasechko, S., Taylor, R.G., 2015. Intensive rainfall recharges tropical groundwaters. Environmental Research Letters 10. https://doi.org/10.1088/1748-9326/10/12/124015

Kurita, N., Ichiyanagi, K., Matsumoto, J., Yamanaka, M.D., Ohata, T., 2009. The relationship between the isotopic content of precipitation and the precipitation amount in tropical regions. Journal of Geochemical Exploration 102, 113–122. https://doi.org/10.1016/j.gexplo.2009.03.002

Lafore, J. -P., Flamant, C., Guichard, F., Parker, D.J., Bouniol, D., Fink, A.H., Giraud, V., Gosset, M., Hall, N., Höller, H., Jones, S.C., Protat, A., Roca, R., Roux, F., Saïd, F., Thorncroft, C., 2011. Progress in understanding of weather systems in West Africa. Atmospheric Science Letters 12, 7–12. https://doi.org/10.1002/asl.335

Landais, A., Risi, C., Bony, S., Vimeux, F., Descroix, L., Falourd, S., Bouygues, A., 2010. Combined measurements of O-17(excess) and d-excess in African monsoon precipitation: Implications for evaluating convective parameterizations. Earth Planet. Sci. Lett. 298, 104–112. https://doi.org/10.1016/j.epsl.2010.07.033

Le Barbé, L., Lebel, T., Tapsoba, D., 2002. Rainfall Variability in West Africa during the Years 1950–90. J. Climate 15, 187–202. https://doi.org/10.1175/1520-0442(2002)015%3C0187:RVIWAD%3E2.0.CO;2

Lloyd, S., 1982. Least squares quantization in PCM. IEEE Trans. Inform. Theory 28, 129–137. https://doi.org/10.1109/TIT.1982.1056489

Luz, B., Barkan, E., 2010. Variations of O-17/O-16 and O-18/O-16 in meteoric waters. Geochim. Cosmochim. Acta 74, 6276–6286. https://doi.org/10.1016/j.gca.2010.08.016

Mahamat Nour, A., Vallet-Coulomb, C., Sylvestre, F., Deschamps, P., 2023. Response of rainfall variability on the evolution of the vegetative cycle in the Chari-Logone basin (Lake Chad basin). J Soil Sci Envir Manag 14, 14–24.

Moore, M., Kuang, Z., Blossey, P.N., 2014. A moisture budget perspective of the amount effect. Geophysical Research Letters 41, 1329–1335. https://doi.org/10.1002/2013GL058302

Munksgaard, N.C., Kurita, N., Sanchez-Murillo, R., Ahmed, N., Araguas, L., Balachew, D.L., Bird, M.I., Chakraborty, S., Chinh, N.K., Cobb, K.M., Ellis, S.A., Esquivel-Hernandez, G., Ganyaglo, S.Y., Gao, J., Gastmans, D., Kaseke, K.F., Kebede, S., Morales, M.R., Mueller, M., Poh, S.C., dos Santos, V., Shaoneng, H., Wang, L., Yacobaccio, H., Zwart, C., 2019. Data Descriptor: Daily observations of stable isotope ratios of rainfall in the tropics. Sci Rep 9, 14419. https://doi.org/10.1038/s41598-019-50973-9

Natali, S., Doveri, M., Giannecchini, R., Baneschi, I., Zanchetta, G., 2022. Is the deuterium excess in precipitation a reliable tracer of moisture sources and water resources fate in the western Mediterranean? New insights from Apuan Alps (Italy). Journal of Hydrology 614, 128497. https://doi.org/10.1016/j.jhydrol.2022.128497

Niang, C., Mancho, A.M., García-Garrido, V.J., Mohino, E., Rodriguez-Fonseca, B., Curbelo, J., 2020. Transport pathways across the West African Monsoon as revealed by Lagrangian Coherent Structures. Sci Rep 10, 12543. https://doi.org/10.1038/s41598-020-69159-9

Nicholson, S.E., 2013. The West African Sahel: A Review of Recent Studies on the Rainfall Regime and Its Interannual Variability. ISRN Meteorology 2013, 1–32. https://doi.org/10.1155/2013/453521

Nicholson, S.E., Funk, C., Fink, A.H., 2018. Rainfall over the African continent from the 19th through the 21st century. Global and Planetary Change 165, 114–127. https://doi.org/10.1016/j.gloplacha.2017.12.014

Nlend, B., Celle-Jeanton, H., Risi, C., Pohl, B., Huneau, F., Boum-Nkot, S.N., Seze, G., Roucou, P., Camberlin, P., Etame, J., Ketchemen-Tandia, B., 2020. Identification of processes that control the stable isotope composition of rainwater in the humid tropical West-Central Africa. J. Hydrol. 584, 124650. https://doi.org/10.1016/j.jhydrol.2020.124650

Pedregosa, F., Pedregosa, F., Varoquaux, G., Varoquaux, G., Org, N., Gramfort, A., Gramfort, A., Michel, V., Michel, V., Fr, L., Thirion, B., Thirion, B., Grisel, O., Grisel, O., Blondel, M., Prettenhofer, P., Prettenhofer, P., Weiss, R., Dubourg, V., Dubourg, V., Vanderplas, J., Passos, A., Tp, A., Cournapeau, D., 2011. Scikit-learn: Machine Learning in Python. Journal of Machine Learning Research 12, 2825–2830.

Pfahl, S., Sodemann, H., 2014. What controls deuterium excess in global precipitation? Clim. Past 10, 771–781. https://doi.org/10.5194/cp-10-771-2014

Risi, C., Bony, S., Vimeux, F., Jouzel, J., 2010. Water-stable isotopes in the LMDZ4 general circulation model: Model evaluation for present-day and past climates and applications to climatic interpretations of tropical isotopic records. Journal of Geophysical Research-Atmospheres 115. https://doi.org/10.1029/2009jd013255

Risi, C., Landais, A., Winkler, R., Vimeux, F., 2013. Can we determine what controls the spatio-temporal distribution of d-excess and^{17}O-excess in precipitation using the LMDZ general circulation model? Clim. Past 9, 2173–2193. https://doi.org/10.5194/cp-9-2173-2013

Risi, C., Muller, C., Vimeux, F., Blossey, P., Védeau, G., Dufaux, C., Abramian, S., 2023. What Controls the Mesoscale Variations in Water Isotopic Composition Within Tropical Cyclones and Squall Lines? Cloud Resolving Model Simulations in Radiative-Convective Equilibrium. J Adv Model Earth Syst 15, e2022MS003331. https://doi.org/10.1029/2022MS003331

Romps, D.M., 2017. Exact Expression for the Lifting Condensation Level. Journal of the Atmospheric Sciences 74, 3891–3900. https://doi.org/10.1175/JAS-D-17-0102.1

Rousseeuw, P.J., 1987. Silhouettes: A graphical aid to the interpretation and validation of cluster analysis. Journal of Computational and Applied Mathematics 20, 53–65. https://doi.org/10.1016/0377-0427(87)90125-7

Rozanski, K., Araguas-Araguas, L., Gonfiantini, R., 1993. Isotopic Patterns in Modern Global Precipitation, in: al., P.K.S. et (Ed.), Climate Change in Continental Isotopic Records, Geophysical Monograph 78. AGU, Washington, D.C., pp. 1–36.

Schneider, T., Bischoff, T., Haug, G.H., 2014. Migrations and dynamics of the intertropical convergence zone. Nature 513, 45–53. https://doi.org/10.1038/nature13636

Schoenemann, S.W., Schauer, A.J., Steig, E.J., 2013. Measurement of SLAP2 and GISP 17O and proposed VSMOW-SLAP normalization for 17O and 17Oexcess. Rapid Commun. Mass Spectrom. 27, 582–590. https://doi.org/10.1002/rcm.6486

https://doi.org/10.5194/egusphere-2026-5233
Preprint. Discussion started: 14 September 2026

Scholl, M.A., Shanley, J.B., Zegarra, J.P., Coplen, T.B., 2009. The stable isotope amount effect: New insights from NEXRAD echo tops, Luquillo Mountains, Puerto Rico. Water Resources Research 45, 2008WR007515. https://doi.org/10.1029/2008WR007515

Sodemann, H., Schwierz, C., Wernli, H., 2008. Interannual variability of Greenland winter precipitation sources: Lagrangian moisture diagnostic and North Atlantic Oscillation influence. J. Geophys. Res. 113, 2007JD008503. https://doi.org/10.1029/2007JD008503

Stein, A.F., Draxler, R.R., Rolph, G.D., Stunder, B.J.B., Cohen, M.D., Ngan, F., 2015. NOAA's HYSPLIT Atmospheric Transport and Dispersion Modeling System. Bulletin of the American Meteorological Society 96, 2059–2077. https://doi.org/10.1175/BAMS-D-14-00110.1

Sultan, B., Janicot, S., 2003. The West African Monsoon Dynamics. Part II: The "Preonset" and "Onset" of the Summer Monsoon. J. Climate 16, 3407–3427. https://doi.org/10.1175/1520-0442(2003)016%3C3407:TWAMDP%3E2.0.CO;2

Sun, C., Shanahan, T., He, S., Bailey, A., Nusbaumer, J., Hu, J., Hillman, A., Ornouski, E., Warner, J., Delong, K., 2024. 17O-Excess in Tropical Cyclones Reflects Local Rain Re-Evaporation More Than Moisture Source Conditions. J. Geophys. Res.-Atmos. 129, e2023JD039361. https://doi.org/10.1029/2023JD039361

Surma, J., Assonov, S., Staubwasser, M., 2021. Triple Oxygen Isotope Systematics in the Hydrologic Cycle. Reviews in Mineralogy and Geochemistry 86, 401–428. https://doi.org/10.2138/rmg.2021.86.12

Taupin, J.D., Coudrain-Ribstein, A., Gallaire, R., Zuppi, G.M., Filly, A., 2000. Rainfall characteristics (18O, 2H, dT, dHr) in western Africa: regional scale and influence of irrigated areas. Journal of Geophysical Research 105, 11911–11924.

Taylor, C.M., Belušić, D., Guichard, F., Parker, D.J., Vischel, T., Bock, O., Harris, P.P., Janicot, S., Klein, C., Panthou, G., 2017. Frequency of extreme Sahelian storms tripled since 1982 in satellite observations. Nature 544, 475–478. https://doi.org/10.1038/nature22069

Taylor, C.M., Parker, D.J., Kalthoff, N., Gaertner, M.A., Philippon, N., Bastin, S., Harris, P.P., Boone, A., Guichard, F., Agusti-Panareda, A., Baldi, M., Cerlini, P., Descroix, L., Douville, H., Flamant, C., Grandpeix, J., Polcher, J., 2011. New perspectives on land–atmosphere feedbacks from the African Monsoon Multidisciplinary Analysis. Atmospheric Science Letters 12, 38–44. https://doi.org/10.1002/asl.336

Terzer-Wassmuth, S., Araguas-Araguas, L.J., Wassenaar, L.I., Stumpp, C., 2023. Global and local meteoric water lines for δ17O/δ18O and the spatiotemporal distribution of Δ′17O in Earth's precipitation. Sci Rep 13, 19056. https://doi.org/10.1038/s41598-023-45920-8

Tharammal, T., Bala, G., Noone, D., 2017. Impact of deep convection on the isotopic amount effect in tropical precipitation. J. Geophys. Res.-Atmos. 122, 1505–1523. https://doi.org/10.1002/2016JD025555

Thorncroft, C.D., Nguyen, H., Zhang, C., Peyrillé, P., 2011. Annual cycle of the West African monsoon: regional circulations and associated water vapour transport. Quart J Royal Meteoro Soc 137, 129–147. https://doi.org/10.1002/qj.728

Thorndike, R.L., 1953. Who Belongs in the Family? Psychometrika 18, 267–276. https://doi.org/10.1007/BF02289263

Tremoy, G., Vimeux, F., Soumana, S., Souley, I., Risi, C., Favreau, G., Oi, M., 2014. Clustering mesoscale convective systems with laser-based water vapor delta O-18 monitoring in Niamey (Niger). Journal of Geophysical Research-Atmospheres 119, 5079–5103. https://doi.org/10.1002/2013JD020968

Uechi, Y., Uemura, R., 2019. Dominant influence of the humidity in the moisture source region on the 17O-excess in precipitation on a subtropical island. Earth and Planetary Science Letters 513, 20–28. https://doi.org/10.1016/j.epsl.2019.02.012

Vallet-Coulomb, C., Couapel, M., Sonzogni, C., 2021. Improving memory effect correction to achieve high-precision analysis of $\delta^{17}O$, $\delta^{18}O$, $\delta^{2}H$, ^{17}O-excess and d-excess in water using cavity ring-down laser spectroscopy. Rapid Comm Mass Spectrometry 35, e9108. https://doi.org/10.1002/rcm.9108

Vallet-Coulomb, C., Gasse, F., Sonzogni, C., 2008. Seasonal evolution of the isotopic composition of atmospheric water vapour above a tropical lake: Deuterium excess and implication for water recycling. Geochimica et Cosmochimica Acta 72, 4661–4674. https://doi.org/10.1016/j.gca.2008.06.025

Voigt, C., Alexandre, A., Reiter, I.M., Orts, J.-P., Vallet-Coulomb, C., Piel, C., Mazur, J.-C., Aleman, J., Sonzogni, C., Miche, H., 2022. 17O-excess of grass phytoliths record daytime air relative humidity at a natural Mediterranean site. Biogeosci. Discuss. 1.

Voigt, C., Vallet-Coulomb, C., Piel, C., Sauze, J., Reiter, I.M., Orts, J.-P., Chalié, F., Cassou, C., Xueref-Remy, I., Alexandre, A., 2026. Drivers of diurnal and seasonal dynamics of triple oxygen isotopes in atmospheric water vapor and precipitation at a Mediterranean forest site. Atmos. Chem. Phys. 26, 9295–9335. https://doi.org/10.5194/acp-26-9295-2026

Warner, M.S.C., 2018. Introduction to PySPLIT: A Python Toolkit for NOAA ARL's HYSPLIT Model. Comput. Sci. Eng. 20, 47–62. https://doi.org/10.1109/MCSE.2017.3301549

https://doi.org/10.5194/egusphere-2026-5233
Preprint. Discussion started: 14 September 2026

Wei, Z., Lee, X., Liu, Z., Seeboonruang, U., Koike, M., Yoshimura, K., 2018. Influences of large-scale convection and moisture source on monthly precipitation isotope ratios observed in Thailand, Southeast Asia. Earth Planet. Sci. Lett. 488, 181–192. https://doi.org/10.1016/j.epsl.2018.02.015

Xia, Z., 2023. Quantifying the Fingerprint of Oceanic Moisture Source Conditions in Deuterium and 17O Excess Parameters of Precipitation. Geophys. Res. Lett. 50, e2022GL101901. https://doi.org/10.1029/2022GL101901

Xia, Z., Surma, J., Winnick, M.J., 2023. The response and sensitivity of deuterium and 17O excess parameters in precipitation to hydroclimate processes. Earth-Sci. Rev. 242, 104432. https://doi.org/10.1016/j.earscirev.2023.104432

Xia, Z., Winnick, M.J., 2021. The competing effects of terrestrial evapotranspiration and raindrop re-evaporation on the deuterium excess of continental precipitation. Earth and Planetary Science Letters 572, 117120. https://doi.org/10.1016/j.epsl.2021.117120

Xu, W., Zipser, E.J., 2012. Properties of deep convection in tropical continental, monsoon, and oceanic rainfall regimes. Geophysical Research Letters 39, 2012GL051242. https://doi.org/10.1029/2012GL051242

Yoshimura, K., 2015. Stable Water Isotopes in Climatology, Meteorology, and Hydrology: A Review. Journal of the Meteorological Society of Japan 93, 513–533. https://doi.org/10.2151/jmsj.2015-036

Yoshimura, K., Kanamitsu, M., Noone, D., Oki, T., 2008. Historical isotope simulation using Reanalysis atmospheric data. J. Geophys. Res. 113, 2008JD010074. https://doi.org/10.1029/2008JD010074

Yu, W., Guo, R., Thompson, L.G., Zhang, J., Lewis, S., Jing, Z., He, J., Ma, Y., Xu, B., Wu, G., Zhou, X., Tang, W., Wang, Q., Ren, P., Zhang, Z., Qu, D., 2024. Water isotope ratios reflect convection intensity rather than rain type proportions in the pantropics. Sci. Adv. 10, eado3258. https://doi.org/10.1126/sciadv.ado3258

Yu, Y., Notaro, M., Wang, F., Mao, J., Shi, X., Wei, Y., 2017. Observed positive vegetation-rainfall feedbacks in the Sahel dominated by a moisture recycling mechanism. Nat Commun 8, 1873. https://doi.org/10.1038/s41467-017-02021-1

Zhan, Z., Pang, H., Wu, S., Liu, Z., Zhang, W., Xu, T., Cheng, H., Hou, S., 2023. Determining key upstream convection and rainout zones affecting δ18O in water vapor and precipitation based on 10-year continuous observations in the East Asian Monsoon region. Earth and Planetary Science Letters 601, 117912. https://doi.org/10.1016/j.epsl.2022.117912

Zhang, Y., He, S., Wee, B., LeGrande, A.N., Wang, J., Goodkin, N., Wang, X., 2024. Precipitation 17O-Excess Altered During Tropical Convection: Evidence From Monsoon Cold Surges in Singapore. J. Geophys. Res.-Atmos. 129, e2023JD040437. https://doi.org/10.1029/2023JD040437